Istituto Universitario
di Studi Superiori di Pavia

Università degli Studi
di Pavia

ROSE School

EUROPEAN SCHOOL FOR ADVANCED STUDIES IN REDUCTION OF SEISMIC RISK

An Isogeometric Analysis Approach for the Study of Structural Vibrations

A Thesis Submitted in Partial

Fulfilment of the Requirements for the Master Degree in

EARTHQUAKE ENGINEERING

By

ALESSANDRO REALI

Supervisors: Prof. THOMAS J.R. HUGHES
Prof. FERDINANDO AURICCHIO

Pavia, October 2004

The dissertation entitled "An Isogeometric Analysis Approach for the Study of Structural Vibrations", by Alessandro Reali, has been approved in partial fulfilment of the requirements for the Master Degree in Earthquake Engineering.

Thomas J.R. Hughes _____

Ferdinando Auricchio _____

ABSTRACT

The concept of Isogeometric Analysis recently introduced by Hughes et al. (2004) is for the first time applied to the study of structural vibrations.
In this framework, the good behaviour of the method is verified and compared with some classical finite element results. Numerical experiments are shown for structural one-, two- and three-dimensional problems in order to test the performances of this promising technique in the field of the analysis of natural frequencies and modes.

Keywords: NURBS, isogeometric analysis, structural vibrations, discrete spectrum, finite element analysis, rotation-free bending elements, weak boundary conditions

ACKNOWLEDGEMENTS

I want to thank Professor Tom Hughes to have given me the great opportunity to be part of his team in these months. I started to know Finite Elements through his book and working with him was indeed beyond my professional desires. Well, it happened, and I have to say that it has been really a fantastic and fruitful unexpected experience.
I thank Professor Ferdinando Auricchio for the confidence in me that he has always shown and for all the years that I have spent (and, hopefully, I will spend) working with him. I really have learnt more than a lot from him.
I also wish to thank Professor Gian Michele Calvi and his collaborators for starting and supporting the stimulating environment which ROSE School is.
Thanks to my mom, my dad, Federica, Elisa and Baldo, and all the members of my family (and I mean also Rita and Francesco), both here and in Heaven: without their love and constant support it would have been impossible every step up to now.
I thank so much also my friends: all of them have played an important role in my life. In particular I want to thank here my "ROSE" friends Chiara, Davide, Giorgio, Iunio, Maria, Paola, Paolo, Sandra, Simone and all those who have shared with me this period, because they have made studying together an exciting experience.
Finally I want to thank the most important person in my life, my wife Paola, because she is the real sense of what I do, every day. I have missed her so much in these months far away and I know that she has missed me too, especially in one of the hardest period of her life. I will not leave her alone any more in our walking together, even if she knows that everywhere she is there is my heart.

Austin (Texas), October 2004

AN ISOGEOMETRIC ANALYSIS APPROACH FOR THE STUDY OF STRUCTURAL VIBRATIONS

CONTENTS

LIST OF TABLES

LIST OF FIGURES

1. INTRODUCTION

The Isogeometric Analysis concept has been recently introduced by Hughes et al. (2004) in the framework of structural and fluids analysis; for the first time, in this work I investigate the possibilities of this new method when applied to structural vibrations.

The Isogeometric Analysis consists in an isoparametric analysis approach where basis functions generated from Non-Uniform Rational B-Splines (commonly referred to as NURBS) are employed in order to describe both the geometry and the unknown variables of the problem. Its name ("isogeometric") is due to the fact that the use of NURBS leads to an exact geometric description of the domain, while in standard finite element analysis it is necessary to approximate it by means of a mesh. Note that with "exact" I mean "as exact as CAD modeling can be", because NURBS are the standard functions for describing and modeling objects in CAD. A very interesting example is that, by employing NURBS, every kind of conic section can be constructed exactly (see Piegl and Tiller (1997) and Rogers (2001)).
The fact that even the coarsest mesh retains exact geometry makes possible a direct refinement, without going back to the CAD model from which the mesh has been generated; finite element analysis, instead, needs to interact with the CAD system at every refinement step, except that for very simple geometries.
Moreover, besides the equivalents of classical finite element h- and p-refinements, another higher-continuity refinement strategy, named k-refinement, is possible.
Among the many advantages arising from this NURBS-based approach and highlighted in Hughes et al. (2004), some properties as the high-order continuity of the bases and the mass matrix point-wise positivity seem to be very suitable and promising for frequency analysis.
So my goal is to investigate the behaviour of this new approach in the context of the structural

eigenvalue problems.

I want to stress here that, in general, also Isogeometric Analysis approaches not based on Non-Uniform Rational B-Splines can be constructed. However, as NURBS are the most widespread used functions in CAD technology, in this work we only consider NURBS-based Isogeometric Analysis.

2. ORGANIZATION OF THE WORK

The present work is organized in five main Chapters.
The first one consists of a brief introduction to NURBS and Isogeometric Analysis.
In the second one the basic equations of structural vibration theory are summarized.
The third main Chapter refers to 1D problems: the numerical spectra of rod and beam elements obtained using the new method are studied.
Analogously, in the fourth one 2D problems (membrane and plate elements) are studied.
In the last Chapter, finally, some numerical experiments on a circular thin plate, studied by means of 3D solid elements, are presented.

3. NURBS AND ISOGEOMETRIC ANALYSIS

Non-Uniform Rational B-Splines (NURBS) are the standard for describing and modeling curves and surfaces in computer aided design (CAD) and computer graphics. So these functions are widely described in CAD and computer graphics literature (refer for instance to Piegl and Tiller (1997) and to Rogers (2001)) and the aim of this Section is not giving an analytical and algorithmic description of them; here I just want to introduce them briefly and to present the guidelines of Isogeometric Analysis, for which an extensive account has been given by Hughes et al. (2004).

3.1 B-SPLINES

B-Splines are piece-wise polynomial curves whose components are defined as the linear combination of B-Spline basis functions and the components of some points in the space, referred to as *control points*. Fixed the *order* of the B-Spline (i.e. the degree of polynomials), in order to construct the basis functions we have to introduce the so-called *knot vector*, which is a fundamental ingredient for this operation.

3.1.1 Knot Vectors

A *knot vector* Ξ is a set of non-decreasing real numbers representing a set of coordinate in the parametric space of the curve:

$$\Xi = [\xi_1, ..., \xi_{n+p+1}],$$

where p is the order of the B-Spline and n is the number of basis functions (and control points) necessary to describe it.
A knot vector is said to be *uniform* if its knots are equally spaced and *non-uniform* otherwise. Moreover, a knot vector is said to be *open* if its first and last knots are repeated $p+1$ times.
In the following we always deal with *open knot vectors*. An important property of theirs is that basis functions formed from open knot vectors are interpolatory at the ends of the parametric space interval $[\xi_1, \xi_{n+p+1}]$, but not, in general, in correspondence of interior knots.

3.1.2 Basis Functions

Given a knot vector Ξ, B-Spline basis functions are defined recursively starting with $p = 0$ (piece-wise constant basis functions) as:

$$N_{i,0}(\xi) = \begin{cases} 1 \text{ if } \xi_i \leq \xi < \xi_{i+1} \\ 0 \text{ otherwise,} \end{cases} \tag{3.1}$$

and for $p \geq 1$ as:

$$N_{i,p}(\xi) = \frac{\xi - \xi_i}{\xi_{i+p} - \xi_i} N_{i,p-1}(\xi) + \frac{\xi_{i+p+1} - \xi}{\xi_{i+p+1} - \xi_{i+1}} N_{i+1,p-1}(\xi). \tag{3.2}$$

In Figure 3.1 we report as an example the $n = 9$ cubic basis functions generated from the open knot vector $\Xi = [0, 0, 0, 0, 1/6, 1/3, 1/2, 2/3, 5/6, 1, 1, 1, 1]$.

An important property of these functions is that they are C^{p-1}-continuous, if internal knots are not repeated. If a knot has multiplicity k, the function is C^{p-k}-continuous in correspondence of that knot. In particular, when a knot has multiplicity p, the basis function is C^0 and interpolatory at that location.

Other remarkable properties are:

- B-Spline basis functions from an open knot vector constitute a partition of unity: $\sum_{i=1}^{n} N_{i,p}(\xi) = 1 \ \forall \xi$.
- The support of each $N_{i,p}$ is compact and contained in the interval $[\xi_i, \xi_{i+p+1}]$.
- B-Spline basis functions are non-negative: $N_{i,p} \geq 0 \ \forall \xi$.

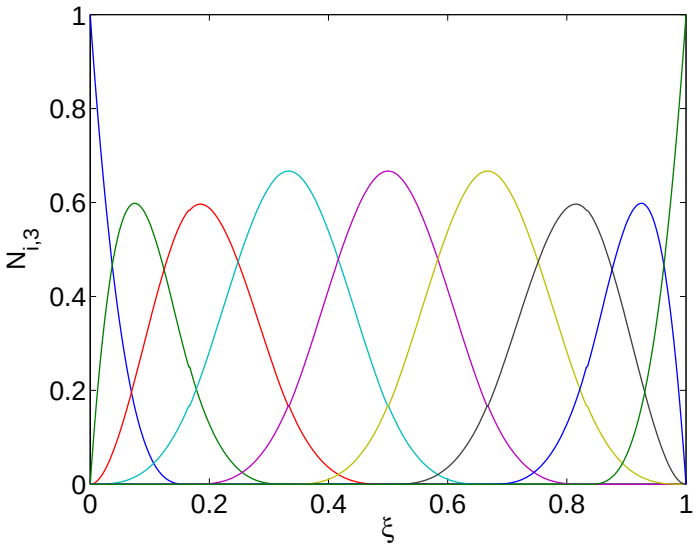

Figure 3.1: Cubic basis functions from an open knot vector.

3.1.3 B-Spline Curves

We have seen that, given the order of the desired B-Spline and a knot vector, it is possible to construct n basis functions. Now, given a set of n points in $\mathbb{R}^d$, referred to as *control points*, we can obtain the components of the piece-wise polynomial B-Spline curve $\mathbf{C}(\xi)$ of order p by taking the linear combination of the basis functions weighted by the components of control points, so:

$$\mathbf{C}(\xi) = \sum_{i=1}^{n} N_{i,p}(\xi)\mathbf{B}_i, \tag{3.3}$$

where $\mathbf{B}_i$ is the i^{th} control point.
The piece-wise linear interpolation of the control points is called *control polygon*.
In Figure 3.2 we report, together with its control polygon, a cubic 2D B-Spline curve generated with the basis functions shown in Figure 3.1.

We remark that a B-Spline curve has continuous derivatives of order $p-1$, which can be decreased by k if a knot or a control point has multiplicity $k+1$.
A very important property of these curves is the so-called *affine covariance*, which consists in the fact that an affine transformation of the curve is obtained by applying the transformation to its control points.

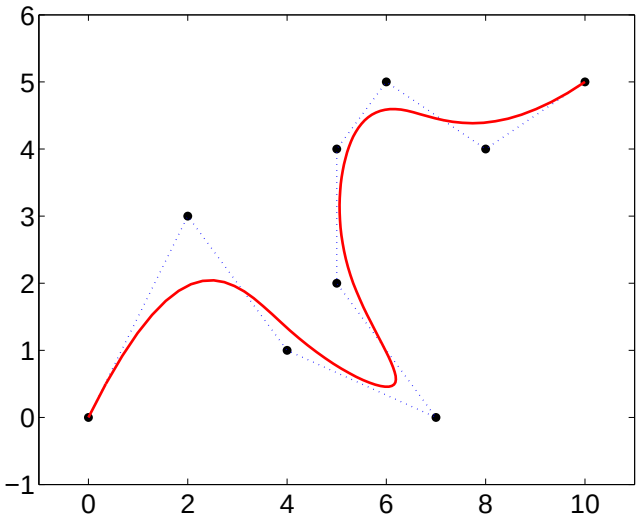

Figure 3.2: Piece-wise cubic B-Spline curve (solid line) and its control polygon (dotted).

3.1.4 B-Spline Surfaces

By means of tensor products, B-Spline surfaces can be constructed starting from a net of $n \times m$ control points $\mathbf{B}_{i,j}$ (*control net*) and knot vectors:

$$\Xi = [\xi_1, ..., \xi_{n+p+1}] \text{ and } \mathrm{H} = [\eta_1, ..., \eta_{m+q+1}].$$

Defined from the two knot vectors the 1D basis functions $N_{i,p}$ and $M_{j,q}$ (with $i = 1, ..., n$ and $j = 1, ..., m$) of order p and q respectively, the B-Spline surface is then constructed as:

$$\mathbf{S}(\xi, \eta) = \sum_{i=1}^{n} \sum_{j=1}^{m} N_{i,p}(\xi) M_{j,q}(\eta) \mathbf{B}_{i,j}. \tag{3.4}$$

3.1.5 B-Spline Solids

By means of tensor products, also B-Spline solids can be constructed. Given an $n \times m \times l$ control net and three knot vectors:

$$\Xi = [\xi_1, ..., \xi_{n+p+1}],\ \mathrm{H} = [\eta_1, ..., \eta_{m+q+1}] \text{ and } \mathrm{Z} = [\zeta_1, ..., \zeta_{l+r+1}],$$

from which the 1D basis functions $N_{i,p}$, $M_{j,q}$ and $L_{k,r}$ (with $i = 1, ..., n$, $j = 1, ..., m$ and $k = 1, ..., l$) of order p, q and r respectively are defined, the B-Spline solid is then:

$$\mathbf{S}(\xi, \eta, \zeta) = \sum_{i=1}^{n} \sum_{j=1}^{m} \sum_{k=1}^{l} N_{i,p}(\xi) M_{j,q}(\eta) L_{k,l}(\zeta) \mathbf{B}_{i,j,k}. \tag{3.5}$$

3.2 NON-UNIFORM RATIONAL B-SPLINES

A rational B-Spline in $\mathbb{R}^d$ is the projection of a non-rational (polynomial) B-Spline defined in $(d+1)$-dimensional homogeneous coordinate space back into d-dimensional physical space (for a complete discussion of these space projections see Rogers (2001) and the references therein). In this way a great variety of geometric entities can be constructed and in particular conic sections can be obtained exactly.
The projective transformation of a B-Spline curve yields a rational polynomial and this is the reason for the name "rational" B-Splines.

To obtain a NURBS curve in $\mathbb{R}^d$, we have to start from a set $\mathbf{B}_i^w$ $(i = 1, ..., n)$ of control points ("projective points") for a B-Spline curve in $\mathbb{R}^{d+1}$ with knot vector Ξ. Then the control points for the NURBS curve are:

$$(\mathbf{B}_i)_j = \frac{(\mathbf{B}_i^w)_j}{(\mathbf{B}_i^w)_{d+1}},\ j = 1, ..., d \tag{3.6}$$

where $(\mathbf{B}_i)_j$ is the j^{th} component of the vector $\mathbf{B}_i$ and $w_i = (\mathbf{B}_i^w)_{d+1}$ is referred to as the i^{th} *weight*.

The NURBS basis functions of order p are then defined as:

$$R_i^p(\xi) = \frac{N_{i,p}(\xi)w_i}{\sum_{\hat{i}=1}^n N_{\hat{i},p}(\xi)w_{\hat{i}}} \tag{3.7}$$

and their first and second derivatives are:

$$(R_i^p)'(\xi) = \frac{N'_{i,p}(\xi)w_i}{\sum_{\hat{i}=1}^n N_{\hat{i},p}(\xi)w_{\hat{i}}} - \frac{N_{i,p}(\xi)w_i \sum_{\hat{i}=1}^n N'_{\hat{i},p}(\xi)w_{\hat{i}}}{(\sum_{\hat{i}=1}^n N_{\hat{i},p}(\xi)w_{\hat{i}})^2} \tag{3.8}$$

and:

$$\begin{aligned}(R_i^p)''(\xi) = \frac{N''_{i,p}(\xi)w_i}{\sum_{\hat{i}=1}^n N_{\hat{i},p}(\xi)w_{\hat{i}}} + \frac{2N_{i,p}(\xi)w_i(\sum_{\hat{i}=1}^n N'_{\hat{i},p}(\xi)w_{\hat{i}})^2}{(\sum_{\hat{i}=1}^n N_{\hat{i},p}(\xi)w_{\hat{i}})^3} + \\ - \frac{2N'_{i,p}(\xi)w_i \sum_{\hat{i}=1}^n N'_{\hat{i},p}(\xi)w_{\hat{i}} + N_{i,p}(\xi)w_i \sum_{\hat{i}=1}^n N''_{\hat{i},p}(\xi)w_{\hat{i}}}{(\sum_{\hat{i}=1}^n N_{\hat{i},p}(\xi)w_{\hat{i}})^2}.\end{aligned} \tag{3.9}$$

The NURBS curve components are the linear combination of the basis functions weighted by the components of control points:

$$\mathbf{C}(\xi) = \sum_{i=1}^n R_i^p(\xi)\mathbf{B}_i. \tag{3.10}$$

Rational surfaces and solids are defined in an analogous way in terms of the basis functions, respectively:

$$R^{p,q}_{i,j}(\xi,\eta) = \frac{N_{i,p}(\xi)M_{j,q}(\eta)w_{i,j}}{\sum_{\hat{i}=1}^{n}\sum_{\hat{i}=1}^{m} N_{\hat{i},p}(\xi)M_{\hat{j},q}(\eta)w_{\hat{i},\hat{j}}} \tag{3.11}$$

and:

$$R^{p,q,r}_{i,j,k}(\xi,\eta,\zeta) = \frac{N_{i,p}(\xi)M_{j,q}(\eta)L_{k,r}(\zeta)w_{i,j,k}}{\sum_{\hat{i}=1}^{n}\sum_{\hat{i}=1}^{m}\sum_{\hat{k}=1}^{l} N_{\hat{i},p}(\xi)M_{\hat{j},q}(\eta)L_{\hat{k},r}(\zeta)w_{\hat{i},\hat{j},\hat{k}}}. \tag{3.12}$$

In the following, we summarize the most remarkable properties of NURBS:

- NURBS basis functions from an open knot vector constitute a partition of unity: $\sum_{i=1}^{n} R^{p}_{i}(\xi) = 1\ \forall\xi$.
- The continuity and supports of NURBS basis functions are the same as for B-Splines.
- NURBS possess the property of affine covariance.
- If all weights are equal, NURBS become B-Splines.
- NURBS surfaces and solids are the projective transformations of tensor product piece-wise polynomial entities.

3.3 ISOGEOMETRIC ANALYSIS

Hughes et al. (2004) propose the concept of *Isogeometric Analysis* as an *exact geometry* alternative to standard finite element analysis. In the following the guidelines for such a technique are reported:

- A mesh for a NURBS patch is defined by the product of open knot vectors. For example, in 3D a mesh is given by $\Xi \times \mathrm{H} \times \mathrm{Z}$.
- Knot spans subdivide the domain into "elements".
- The support of each basis function consists of a small number of elements.
- The control points associated with the basis functions define the geometry.
- The isoparametric concept is invoked, that is the unknown variables are represented in terms of the basis functions which define the geometry. The coefficients of the basis functions are the degrees-of-freedom, or *control variables*.

- Three different mesh refinement strategies are possible: an analogue of classical FEM h-refinement (by knot insertions), an analogue of classical FEM p-refinement (by degree elevation of the basis functions, easily possible because of their recursive definition) and finally a new possibility referred to as k-refinement (which is a sort of high-order/high-continuity h-refinement).

- The arrays constructed from isoparametric NURBS patches can be assembled into global arrays in the same way as finite elements (see Hughes (2000), Chapter 2). Compatibility of NURBS patches is attained by employing the same NURBS edge and surface representations on both sides of patch interfaces. This gives rise to a standard continuous Galerkin method and a mesh refinement necessarily propagates from patch to patch. There exists also the possibility of employing discontinuous Galerkin methods.

- Dirichlet boundary conditions are applied to the control variables. If they are homogeneous Dirichlet conditions, this results in exact point-wise satisfaction. If they are inhomogeneous, the boundary values must be approximated by functions lying within the NURBS space and this results in a "strong" but approximate satisfaction of the boundary conditions. Constraint equations can be used as a "strong" alternative. Another formulation that can be employed is to impose Dirichlet conditions "weakly" (we will further discuss this point later on). Neumann boundary conditions are satisfied naturally as in standard finite element formulations (see Hughes (2000), Chapters 1 and 2).

When applied to structural analysis, which is the field of interest for the present work, it is possible to verify (as highlighted in Hughes et al. (2004)) that isoparametric NURBS patches represent all rigid body motion and constant strain states exactly. So structures assembled from compatible NURBS patches pass standard "patch tests" (see Hughes (2000), Chapters 3 and 4, for a description of patch tests).

4. STRUCTURAL VIBRATIONS

The goal of this Section is to briefly recall the main equations for structural vibrations; for a complete discussion on the subject refer to Hughes (2000) and to classical books of structural dynamics such as Clough and Penzien (1993) and Chopra (2001).

4.1 NATURAL VIBRATION FREQUENCIES AND MODES

Given a multi-degree-of-freedom structural linear system, the undamped, unforced equations of motion which govern the free vibrations of the system are:

$$\mathbf{M}\ddot{\mathbf{u}} + \mathbf{K}\mathbf{u} = \mathbf{0} \tag{4.1}$$

where $\mathbf{M}$ and $\mathbf{K}$ are, respectively, the consistent mass and the stiffness matrices of the system, $\mathbf{u} = \mathbf{u}(\mathbf{x}, t)$ is the displacement vector and $\ddot{\mathbf{u}} = \dfrac{\mathrm{d}^2\mathbf{u}}{\mathrm{d}t^2}$ is the acceleration vector.
The free vibrations of the system in its n^{th} natural mode can be described (by variable separation) by:

$$\mathbf{u}(\mathbf{x}, t) = \boldsymbol{\phi}_n(\mathbf{x}) q_n(t), \tag{4.2}$$

where $\boldsymbol{\phi}_n$ is the n^{th} natural mode vector and $q_n(t)$ is a harmonic function, depending on the n^{th} natural frequency ω_n, of the form:

$$q_n(t) = A_n \cos(\omega_n t) + B_n \sin(\omega_n t). \tag{4.3}$$

Combining equations (4.2) and (4.3) gives:

$$\mathbf{u}(\mathbf{x}, t) = \boldsymbol{\phi}_n(\mathbf{x})(A_n \cos(\omega_n t) + B_n \sin(\omega_n t)) \tag{4.4}$$

which yields:

$$\ddot{\mathbf{u}} = -\omega_n^2 \mathbf{u}. \tag{4.5}$$

Substituting equation (4.5) into the equations of motion (4.1) gives the following linear system:

$$(\mathbf{K} - \omega_n^2 \mathbf{M})\boldsymbol{\phi}_n q_n = \mathbf{0}. \tag{4.6}$$

Asking for nontrivial solutions of this linear system gives rise to the generalized eigenvalue problem:

$$\det(\mathbf{K} - \omega_n^2 \mathbf{M}) = 0, \tag{4.7}$$

whose solutions are the natural frequencies ω_n (with $n = 1, ..., N$, where N is the number of degrees-of-freedom of the system) associated to the natural modes $\boldsymbol{\phi}_n$. Once a natural frequency ω_n is found, it is possible to compute the corresponding natural mode by solving the following linear system for $\boldsymbol{\phi}_n$:

$$(\mathbf{K} - \omega_n^2 \mathbf{M})\boldsymbol{\phi}_n = \mathbf{0}. \tag{4.8}$$

I remark that the natural modes resulting from (4.8) are defined up to a multiplicative normalization constant. Different standard ways of normalization have been proposed, the most used probably being:

$$\boldsymbol{\phi}_n^T \mathbf{M} \boldsymbol{\phi}_n = 1. \tag{4.9}$$

In conclusion, in order to employ the concepts of Isogeometric Analysis to study structural vibrations, the step to perform are:

1. assemble the stiffness matrix $\mathbf{K}$ as proposed in Hughes et al. (2004);
2. assemble the mass matrix $\mathbf{M}$ in an analogous way;
3. solve the eigenvalue problem (4.7).

Then, if there exists also an interest in computing the natural modes, it is necessary to solve as many linear systems like (4.8) as the desired modes are.

5. ONE-DIMENSIONAL PROBLEMS

In this Section I analyze by means of Isogeometric Analysis two types of 1D structural problems corresponding to the solution of the generalized eigenvalue problems arising from 1D Laplace equation (i.e. structural vibrations of a rod) and from 1D biharmonic equation (i.e. structural vibrations of a beam).
I stress that, even if in 1D problems I do not take advantages at all of the exact geometry capability of the formulation, the high continuity and point-wise non-negativity of the basis functions lead anyway to very good results as shown in the following.
Moreover, I want to remark that in the following examples, due to the simplicity of the geometry, all the weights are equal to 1 (i.e. NURBS basis functions collapse to B-Splines).

5.1 LONGITUDINAL VIBRATIONS OF AN ELASTIC ROD

To begin with, I study the problem (see Hughes (2000), Chapter 7, for details about the formulation) of the natural structural vibrations of an elastic fixed-fixed rod of unit length, whose natural frequencies and modes, assuming unit material parameters, are governed by:

$$\begin{aligned} &u_{,xx} + \omega^2 u = 0 \text{ for } x \in]0,1[\\ &u(0) = u(1) = 0, \end{aligned} \tag{5.1}$$

and for which the exact solution in terms of natural frequencies is:

$$\omega_n = n\pi, \text{ with } n = 1, 2, 3... \tag{5.2}$$

After writing the weak formulation and performing the discretization, a problem of the form of (4.7) is easily obtained.

5.1.1 Numerical Experiments

As a first numerical experiment, the generalized eigenproblem (4.7) has been solved with both FEM and Isogeometric Analysis using quadratic basis functions (note that for linear approximation both of them have exactly the same basis functions, the so called "hat functions"). The resulting natural frequencies ω_n^h are reported in Figure 5.1. They are normalized with respect to the exact solution (5.2) and plotted versus the number of modes n, normalized with respect to the total number of degrees-of-freedom N. To produce the spectra of Figure 5.1, I have employed for both the formulations a number of degrees-of-freedom $N = 999$, in order to get them smooth; they are anyway invariant with N.

Figure 5.1 points out the superior behaviour of NURBS basis function compared with finite

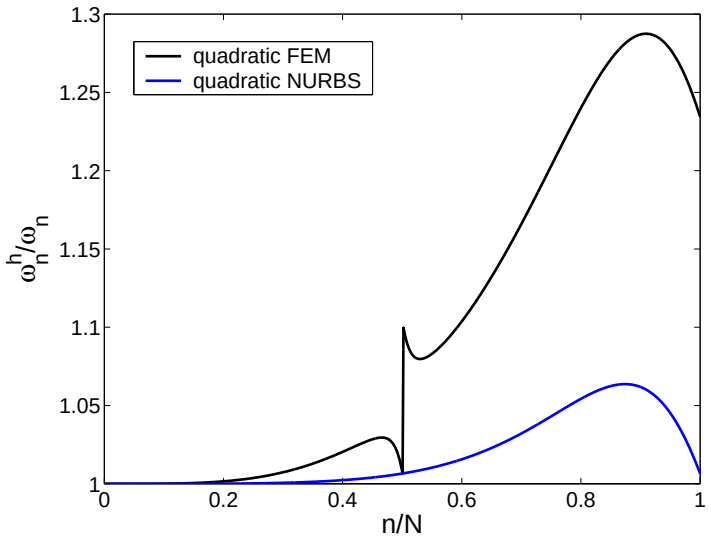

Figure 5.1: Rod problem: normalized discrete spectra using quadratic finite elements and NURBS.

elements, which show a very bad second half of the discrete spectrum. This first result confirm the effectiveness of the idea of employing this new method in structural vibration problems.

I have then performed the same eigenvalue analysis using higher order NURBS basis functions. The resulting discrete spectra are reported in Figure 5.2; the analyses have been carried on using $N = 1000$ degrees-of-freedom (i.e. 1000 control points).

Increasing the order p of the basis functions, the results show higher order of accuracy ($2p$, while standard finite elements achieve $p+1$; see Appendix A for the computation of the order of accuracy using quadratic and cubic NURBS) and decreasing errors. I have to remark, anyway,

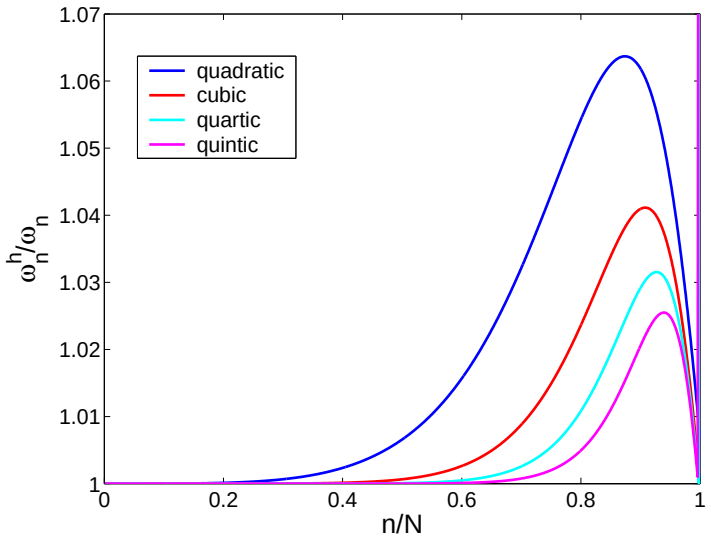

Figure 5.2: Rod problem: normalized discrete spectra using different order NURBS basis functions.

that increasing p also results in the appearance of strange frequencies at the very end of the spectrum, referred to in the following as "outlier frequencies" (in analogy with outlier values in statistics, see for example Motulsky (1995)), whose number and error increase with p. In Figure 5.3, I highlight this behaviour by plotting the last computed frequencies for $p = 2, ..., 10$.

Moreover, in Figure 5.4 I show a plot of the average relative error over the whole spectrum ($\frac{\sum_{n=1}^{N}(\omega_n^h - \omega_n)/\omega_n}{N}$) versus the order p, as compared with the one obtained excluding outlier frequencies from the average ($N = 1000$ control points have been employed).

Finally, Figures 5.5-5.7 show that the order of convergence for frequencies computed using NURBS is $O(h^{2p})$, as with finite elements.

5.1.2 Analytical Determination of the Discrete Spectrum

Following the derivations of Hughes (2000), Chapter 9, it is possible to compute analytically the discrete spectra previously determined numerically.

I start from the mass and stiffness matrices for a generic interior element (notice that for interior elements the basis functions are all the same, see Figure 3.1 as an example, and so the element

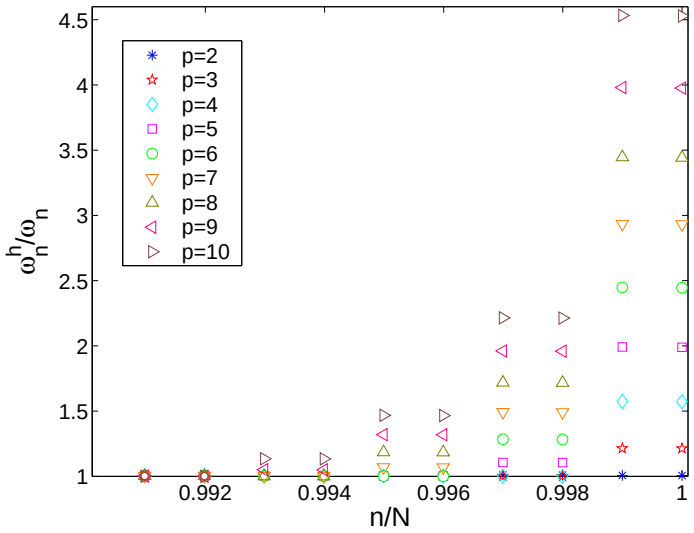

Figure 5.3: Rod problem: last normalized frequencies for $p = 2, ..., 10$.

matrices). Using quadratic NURBS they are respectively:

$$\mathbf{M}^e = \frac{h}{120}\begin{bmatrix} 6 & 13 & 1 \\ 13 & 54 & 13 \\ 1 & 13 & 6 \end{bmatrix} \text{ and } \mathbf{K}^e = \frac{1}{6h}\begin{bmatrix} 2 & -1 & -1 \\ -1 & 2 & -1 \\ -1 & -1 & 2 \end{bmatrix}, \tag{5.3}$$

with $h = 1/n_{el} = 1/(n_{cp} - p)$ (being n_{el} the number of elements, n_{cp} the total number of control points and $p = 2$ the order of the basis functions). Given $\mathbf{M}^e$ and $\mathbf{K}^e$, I can write the scalar equation of motion for the generic interior control point A as:

$$\begin{aligned} &\frac{h}{120}(\ddot{u}_{A-2} + 26\ddot{u}_{A-1} + 66\ddot{u}_A + 26\ddot{u}_{A+1} + \ddot{u}_{A+2}) + \\ &-\frac{1}{6h}(u_{A-2} + 2u_{A-1} - 6u_A + 2u_{A+1} + u_{A+2}) = 0. \end{aligned} \tag{5.4}$$

For compactness, equation (5.4) can be rewritten as:

$$\frac{h^2}{20}\alpha\ddot{u}_A - \beta u_A = 0, \tag{5.5}$$

where α and β are operators working as follows:

$$\begin{aligned} \alpha x_i &= x_{i-2} + 26x_{i-1} + 66x_i + 26x_{i+1} + x_{i+2}, \\ \beta x_i &= x_{i-2} + 2x_{i-1} - 6x_i + 2x_{i+1} + x_{i+2}. \end{aligned} \tag{5.6}$$

Separating the variables as:

$$u_A(t) = \phi_A q(t), \tag{5.7}$$

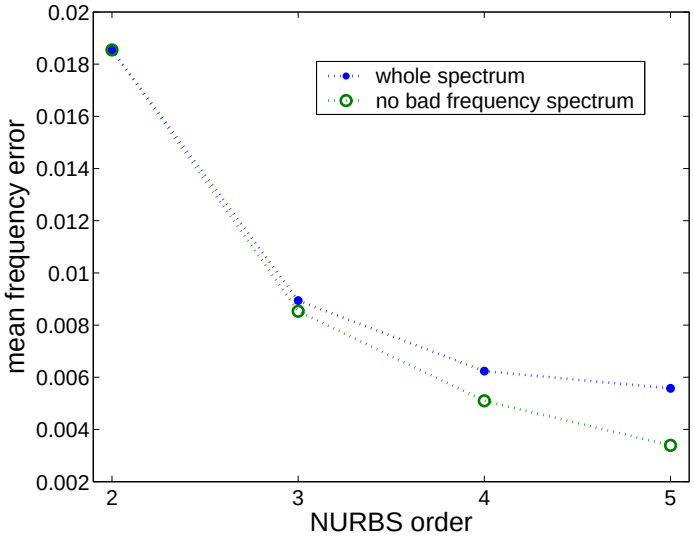

Figure 5.4: Rod problem: average relative error over the whole spectrum (dots) and excluding outlier frequencies (circles).

and substituting this expression into equation (5.5), after adding and subtracting $\frac{(\omega^h h)^2}{20}\alpha u_i$, I obtain:

$$(\ddot{q} + (\omega^h)^2 q)\frac{h^2}{20}\alpha\phi_A - (\frac{(\omega^h h)^2}{20}\alpha\phi_A + \beta\phi_A)q = 0, \tag{5.8}$$

whose satisfaction is achieved by selecting ϕ_A and q such that:

$$(\frac{(\omega^h h)^2}{20}\alpha + \beta)\phi_A = 0 \tag{5.9}$$

and:

$$\ddot{q} + (\omega^h)^2 q = 0. \tag{5.10}$$

Assuming a solution for equation (5.9) of the form (for fixed-fixed boundary conditions):

$$\phi_A = C\sin(A\omega h), \text{ with } \omega = n\pi, \tag{5.11}$$

I can rewrite equation (5.9) as:

$$(\frac{(\omega^h h)^2}{20}\alpha + \beta)\sin(A\omega h) = 0. \tag{5.12}$$

Now, substituting expressions (5.6) for α and β operators and using the trigonometric identity $\sin(a \pm b) = \sin(a)\cos(b) \pm \sin(b)\cos(a)$, I obtain:

$$\frac{(\omega^h h)^2}{20}(16 + 13\cos(\omega h) + \cos^2(\omega h)) - (2 - \cos(\omega h) - \cos^2(\omega h)) = 0, \tag{5.13}$$

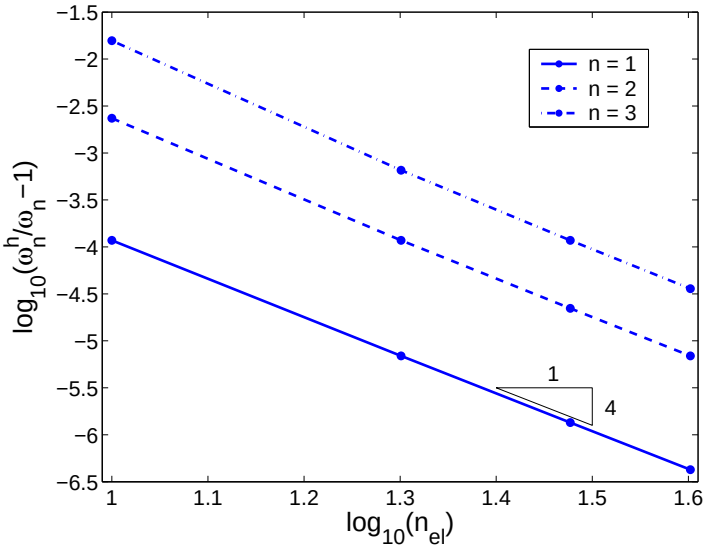

Figure 5.5: Rod problem: order of convergence for the first three frequencies using quadratic NURBS.

which can be solved for $\frac{\omega^h}{\omega}$, giving:

$$\frac{\omega^h}{\omega} = \frac{1}{\omega h}\sqrt{\frac{20(2-\cos(\omega h)-\cos^2(\omega h))}{16+13\cos(\omega h)+\cos^2(\omega h)}}. \tag{5.14}$$

Equation (5.14) is the analytical expression for the normalized discrete spectrum for our problem, computed using quadratic NURBS basis functions.

Analogous calculations can be carried on also for higher order approximations.

In Figure 5.8 we report the analytical and the numerical discrete spectra for quadratic and cubic approximations; for the computation of the numerical discrete spectra, 2000 control points have been employed. It is possible to see that the only differences are in the outlier frequencies at the end of the discrete spectrum obtained using cubic NURBS.

The analytical expression for the discrete spectrum, obtained using cubic NURBS, is:

$$\frac{\omega^h}{\omega} = \frac{1}{\omega h}\sqrt{\frac{42(16-3\cos(\omega h)-12\cos^2(\omega h)-\cos^3(\omega h))}{272+297\cos(\omega h)+60\cos^2(\omega h)+\cos^3(\omega h)}}, \tag{5.15}$$

which has been computed with the same procedure detailed for the quadratic case.

Remark 1:

All the numerical results shown up to now have been obtained using control points computed, starting from the knot vector, with the procedure proposed by Hughes et al. (2004) and referred

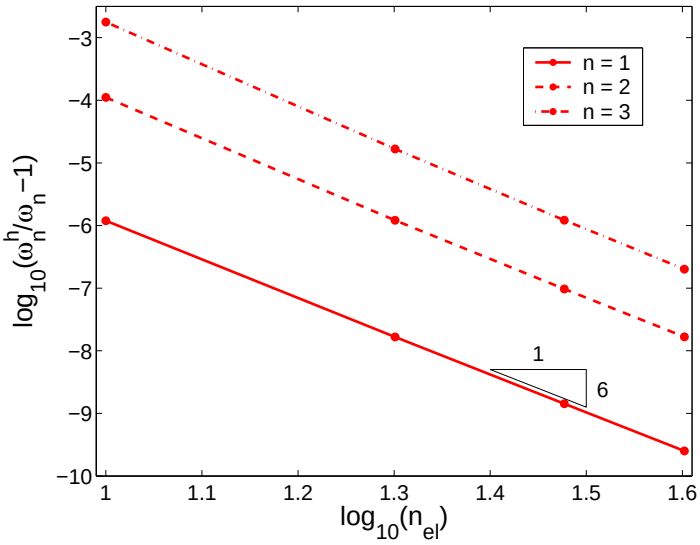

Figure 5.6: Rod problem: order of convergence for the first three frequencies using cubic NURBS.

to as k-refinement. In this way I get a linear parametrization (i.e. constant Jacobian). As seen, the results obtained are very good, except for the presence at the end of the discrete spectrum of what we have called outlier frequencies, which get worse for higher order approximations. A way to avoid this behaviour is to employ equally spaced control points (in Figure 5.9 it is possible to see the difference between the distribution of 21 control points in the case of linear parametrization and of equally spaced points, using cubic NURBS), even if this choice corresponds to a nonlinear parametrization (see Figure 5.10 and 5.11 for a plot of the parametrization $x(\xi)$ and of its Jacobian $J(\xi) = \dfrac{\mathrm{d}x(\xi)}{\mathrm{d}\xi}$ for the cases of equally spaced control points and of linear parametrization corresponding to Figure 5.9).
Finally, Figure 5.12 shows the discrete spectra computed using equally spaced control points: they do not have outlier frequencies and perfectly coincide with the ones computed analytically (and shown in Figure 5.8 for quadratic and cubic NURBS).
However, about this topic more research needs to be done, and it will be the object of future investigations.

Remark 2:

In this work I deal with consistent mass theory, also because I think it to be more suitable than lumped mass when high order approximations are involved.
Anyway, I have performed some tests using lumped mass, too. Figure 5.13 shows that the classical lumped mass formulation, that works well with finite elements, does not work in this

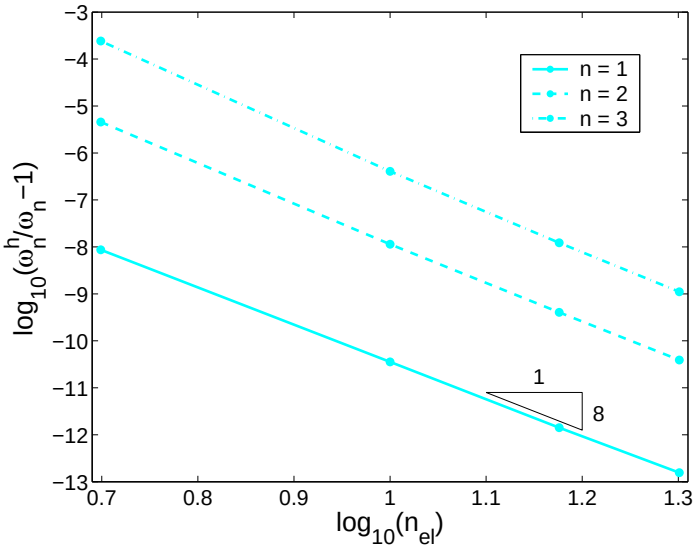

Figure 5.7: Rod problem: order of convergence for the first three frequencies using quartic NURBS.

context. The order of accuracy does not increase with the order p (I have only second order accuracy in each case; see Appendix A for its computation in the quadratic and cubic cases), while errors increase. However, I think that a higher order of accuracy and better results may be achieved employing some special non-uniform knot vector and quadrature scheme choices, in a fashion similar to what is done in Fried and Malkus (1976).
Also about the topic of lumped mass techniques in the framework of Isogeometric Analysis, extensive research still needs to be carried on.

5.2 TRANSVERSAL VIBRATIONS OF AN EULER-BERNOULLI BEAM

Another interesting 1D problem is the natural structural transversal vibrations of a simply-supported, unit length Euler-Bernoulli beam (also about this problem refer to Hughes (2000), Chapter 7, for details about the formulation). For this case, the natural frequencies and modes, assuming unit material parameters, are governed by the following equations:

$$\begin{aligned} &u_{,xxxx} - \omega^2 u = 0 \text{ for } x \in]0,1[\\ &u(0) = u(1) = 0, \end{aligned} \tag{5.16}$$

and the exact solution, in terms of natural frequencies, is:

$$\omega_n = (n\pi)^2, \text{ with } n = 1, 2, 3... \tag{5.17}$$

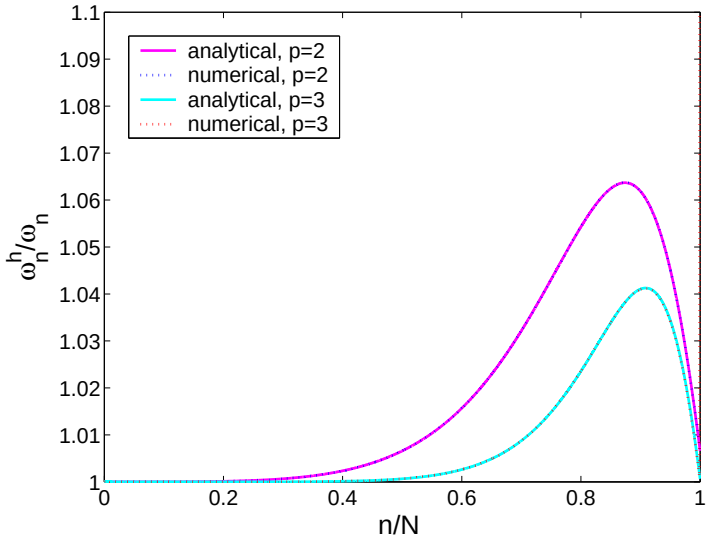

Figure 5.8: Rod problem: analytical versus numerical discrete spectrum computed using quadratic and cubic NURBS.

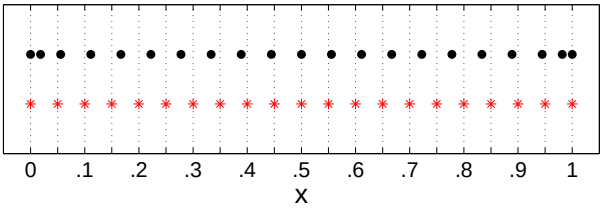

Figure 5.9: Distribution of control points for linear parametrization (dots) as compared with equally spaced control points (asterisks) (cubic NURBS, 21 control points).

Also in this case, after writing the weak formulation and performing the discretization, a problem of the form of (4.7) is obtained.

5.2.1 Numerical Experiments

The numerical experiments performed for the beam problem are analogous (and their results are analogous, too) to the ones reported for the rod.

A remark about the formulation is in order before showing the results: while the classical beam finite element employed to solve problem (5.16) is a 2-node cubic element with two degrees-of-freedom per node (transversal displacement and rotation), my Isogeometric Analysis formulation is rotation-free (see for example Engel et al. (2002)). Later in this Section I will also discuss the problem of the imposition of boundary conditions on rotations.

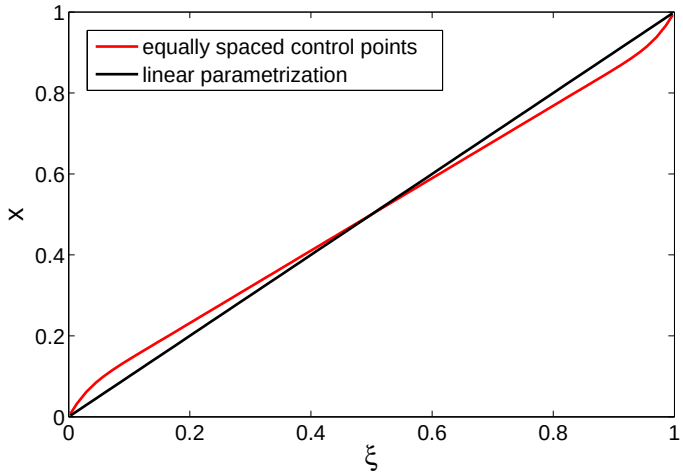

Figure 5.10: Plot of the parametrization for the cases of equally spaced control points and of linear parametrization (cubic NURBS, 21 control points).

In Figure 5.14 I show the discrete spectra obtained using cubic classical finite element and NURBS basis functions. It is seen that the NURBS solution behaves much better, even if also in this case two outlier frequencies are present at the end of the spectrum (even if not clearly evident in the Figure).

Figure 5.15 shows the discrete spectra obtained using different order NURBS basis functions. The behaviour is similar to the one seen in the case of the rod, included outlier frequencies (see Figure 5.16).

In Figure 5.17 I show a plot of the average relative error over the spectrum versus the order p with the exclusion of the outlier frequencies (indeed, their values are so high to make the average over the whole spectrum completely useless; 1000 control points have been employed).

Moreover, Figures 5.18-5.20 show that also here the order of convergence using NURBS is the same as using finite elements, that is $O(h^{2(p-1)})$.

The analytical computation of the discrete spectrum performed for the previous problem can be carried over in the same way as before also in this case. Employing cubic NURBS shape functions, for example, gives rise to the following expression:

$$\frac{\omega^h}{\omega} = \frac{1}{\omega h^2}\sqrt{\frac{210(2-3\cos(\omega h)+\cos^3(\omega h))}{272+297\cos(\omega h)+60\cos^2(\omega h)+\cos^3(\omega h)}}. \tag{5.18}$$

In Figure 5.21 I report the analytical and the numerical discrete spectra for cubic and quartic

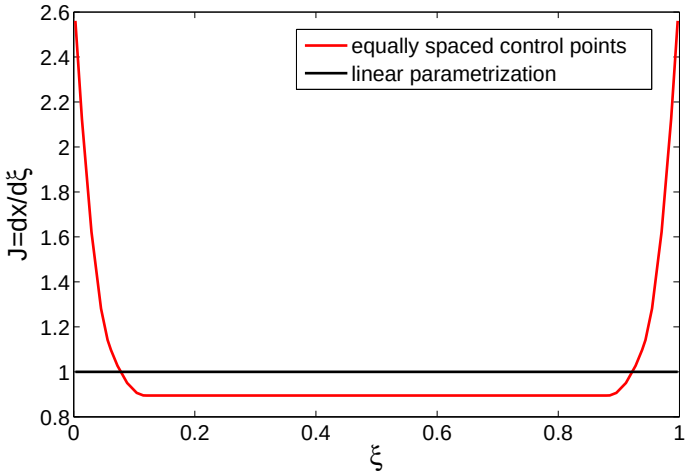

Figure 5.11: Plot of the Jacobian of the parametrization for the cases of equally spaced control points and of linear parametrization (cubic NURBS, 21 control points).

approximations; for the computation of the numerical discrete spectra 2000 control points have been employed. It is possible to see that also in this case the only differences are in the outlier frequencies at the end of the numerical discrete spectra.

As already shown for the rod, this behaviour can be cured by means of a different choice in the distribution of the control points, using, instead of a linear parametrization, a nonlinear one with control points equally spaced. In this way, I obtain the discrete spectra of Figure 5.22, which coincide perfectly with the analytically computed ones and do not show any outlier frequency.

5.2.2 Boundary conditions on rotations

I have already mentioned that the formulation I have employed is rotation-free, in the sense that the only unknowns are the transversal displacements; rotations can be computed as displacement derivatives, but are not approximated as independent variables.
A problem that may arise is that the boundary conditions for a beam frame are usually given also on rotations. For example, if I want to study the natural frequencies of one of the simplest structural member, the cantilever beam, I have to solve the problem (considering unit material parameters):

$$\begin{aligned} &u_{,xxxx} - \omega^2 u = 0 \text{ for } x \in]0,1[\\ &u(0) = u_{,x}(0) = 0, \end{aligned} \tag{5.19}$$

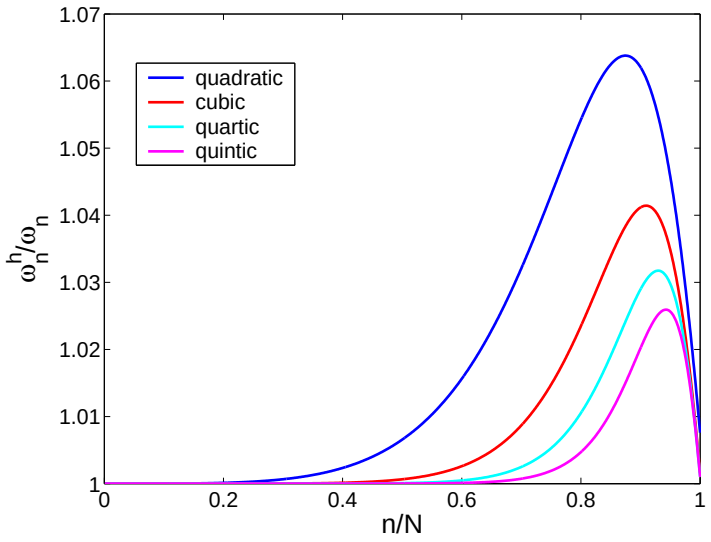

Figure 5.12: Rod problem: normalized discrete spectra using equally spaced control points.

imposing a zero boundary condition on the rotation of the first end $\theta(0) = u_{,x}(0)$. For this example, I take as reference solution the one computed in Chopra (2001), that is, for our unit material parameter choice:

$$\begin{gathered} \omega_n = \beta_n^2, \\ \text{with } \beta_1 = 1.8751,\ \beta_2 = 4.6941,\ \beta_3 = 7.8548,\ \beta_4 = 10.996 \\ \text{and } \beta_n = (n - 1/2)\pi \text{ for } n > 4. \end{gathered} \tag{5.20}$$

In order to solve this problem, I propose here two strategies, one based on a weak boundary condition imposition and the other on the Lagrange multiplier technique.

The former consists in using the formulation suggested in Engel et al. (2002), so that, in my example, I end up with the following expression for the bilinear form A originating the stiffness matrix (which includes the weak form of the boundary condition plus a stabilization term):

$$A(v^h, u^h) = \int_0^1 v^h_{,xx} u^h_{,xx} \mathrm{d}x + v^h_{,x} u^h_{,xx}|_{x=0} + v^h_{,xx} u^h_{,x}|_{x=0} + \tau v_{,x} u_{,x}|_{x=0}, \tag{5.21}$$

where v^h and u^h are the discrete test and unknown functions, respectively, and τ is a stabilization parameter.

In a way analogous to what is done in Prudhomme et al. (2001) in the framework of Poisson problems, it can be shown that the choice of τ needs to be proportional to p^2/h, where p is the order of the NURBS bases employed and $h = 1/n_{el}$ is a mesh parameter (n_{el} is the number of elements used).

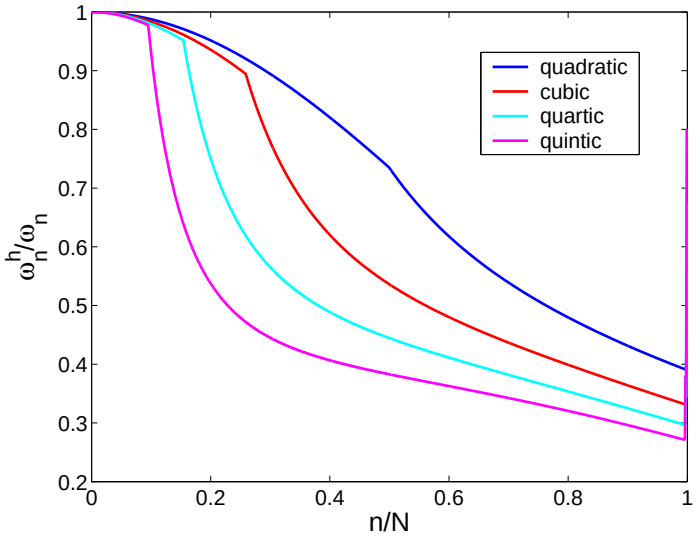

Figure 5.13: Rod problem: normalized discrete spectra using different order NURBS basis functions; lumped mass formulation.

By means of this formulation I have solved the cantilever beam problem (5.19) and the corresponding discrete spectra for different order NURBS are shown in Figure 5.23 (1000 control points and a stabilization parameter $\tau = p^2/h$ have been used).
Figure 5.23 shows the same behaviour seen in Figure 5.15, and also here I have to notice the presence of some outlier frequencies at the end of the spectrum (not evident in Figure 5.23 because of scale choices), which get worse as the order of the bases increases.

The other way to deal with boundary conditions on rotations is the imposition of the constraint through Lagrange multipliers. In this way we obtain the following bilinear form A:

$$A(v^h, u^h) = \int_0^1 v^h_{,xx} u^h_{,xx} \mathrm{d}x + \lambda v^h_{,x}|_{x=0}, \tag{5.22}$$

where λ is the Lagrange multiplier. I have also to add the equation:

$$\mu u^h_{,x}|_{x=0} = 0, \tag{5.23}$$

where μ is the test counterpart of λ.
Obviously this procedure have the disadvantage of introducing extra (unnecessary) variables (the multipliers), but it does not need stabilization.
The numerical results are equivalent to the ones of the weak approach, as Figure 5.24 shows.

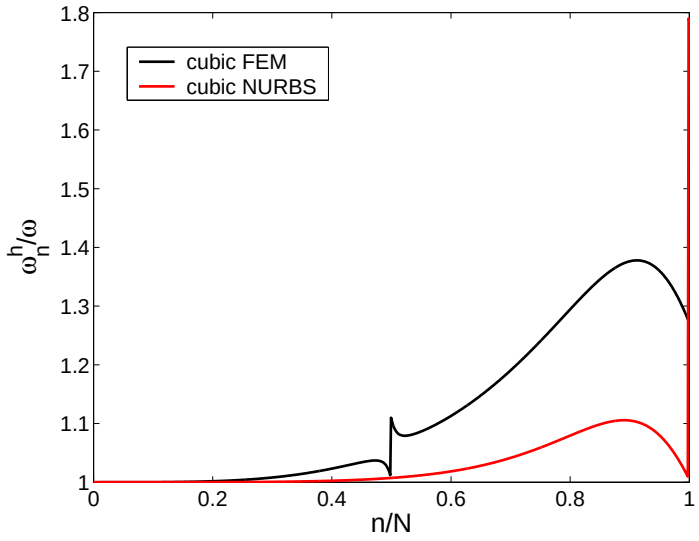

Figure 5.14: Beam problem: normalized discrete spectra using cubic finite elements and NURBS.

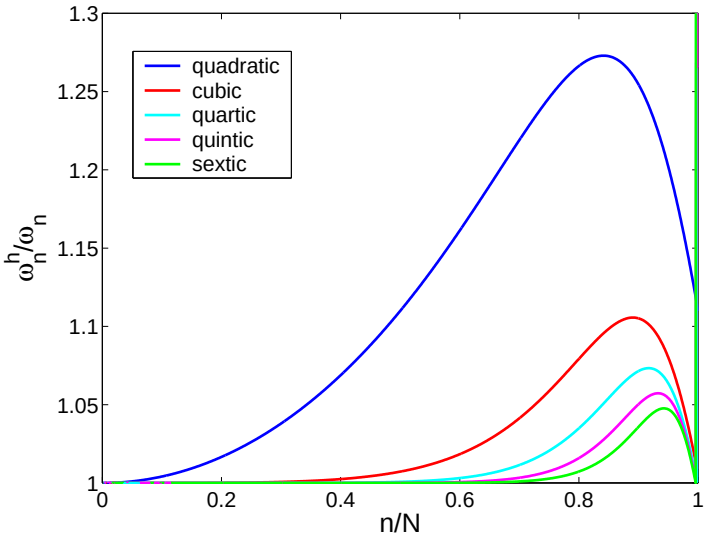

Figure 5.15: Beam problem: normalized discrete spectra using different order NURBS basis functions.

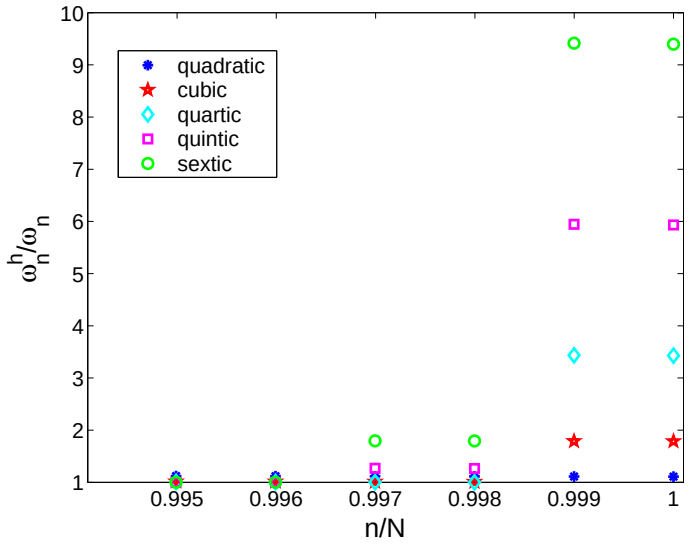

Figure 5.16: Beam problem: last normalized frequencies for $p = 2, ..., 10$.

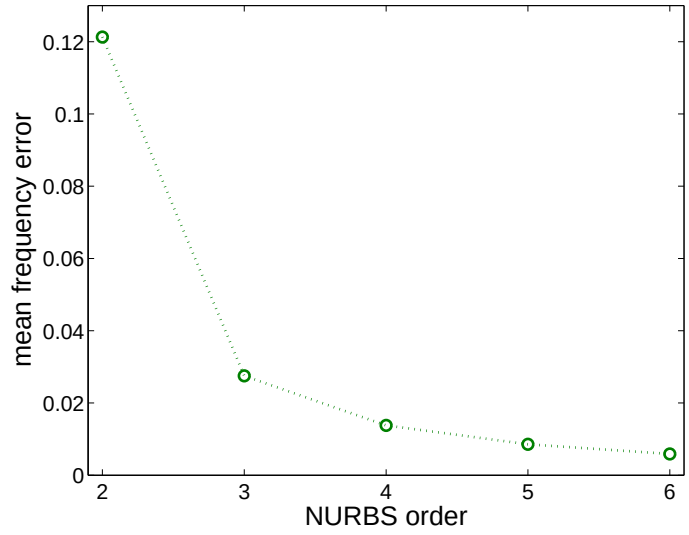

Figure 5.17: Beam problem: average relative error over the spectrum with the exclusion of outlier frequencies.

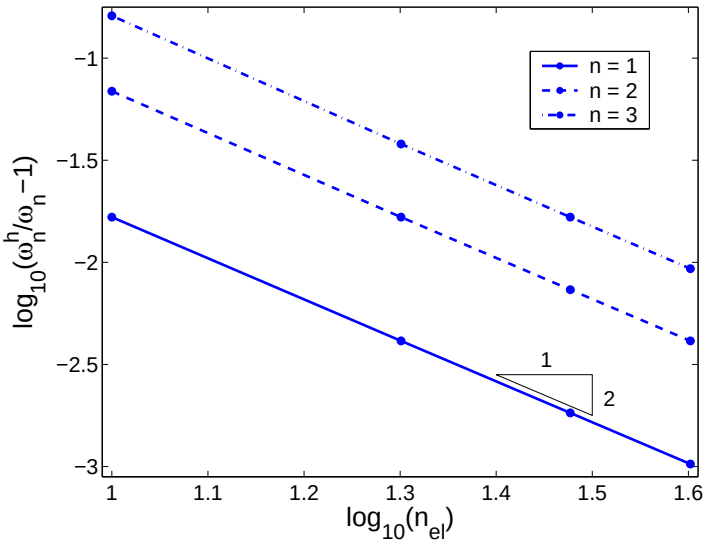

Figure 5.18: Beam problem: order of convergence for the first three frequencies using quadratic NURBS.

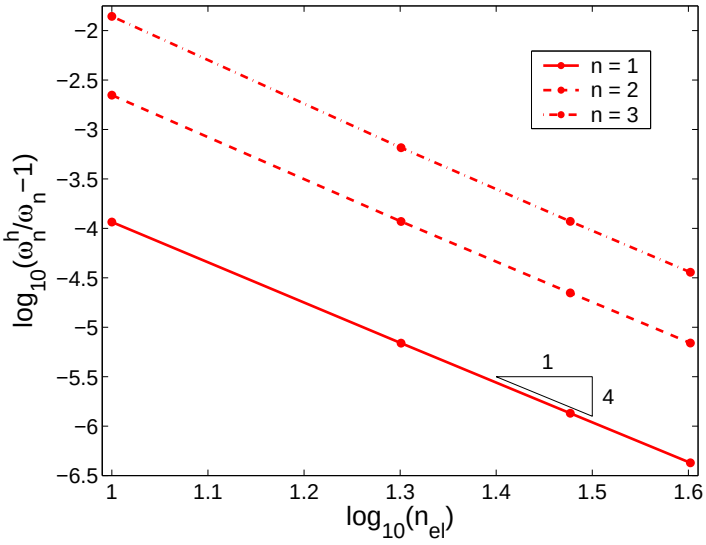

Figure 5.19: Beam problem: order of convergence for the first three frequencies using cubic NURBS.

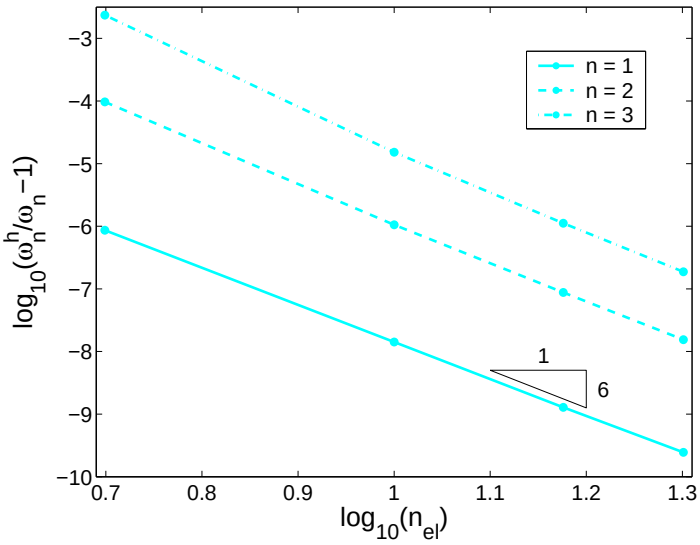

Figure 5.20: Beam problem: order of convergence for the first three frequencies using quartic NURBS.

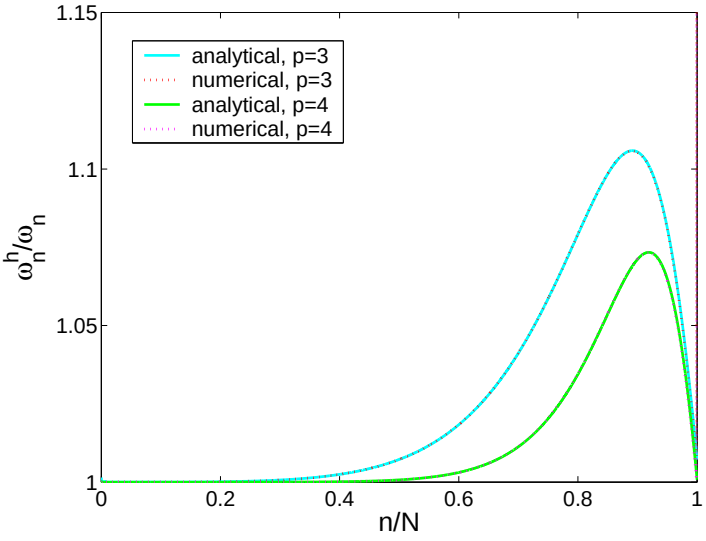

Figure 5.21: Beam problem: analytical versus numerical discrete spectrum computed using cubic and quartic NURBS.

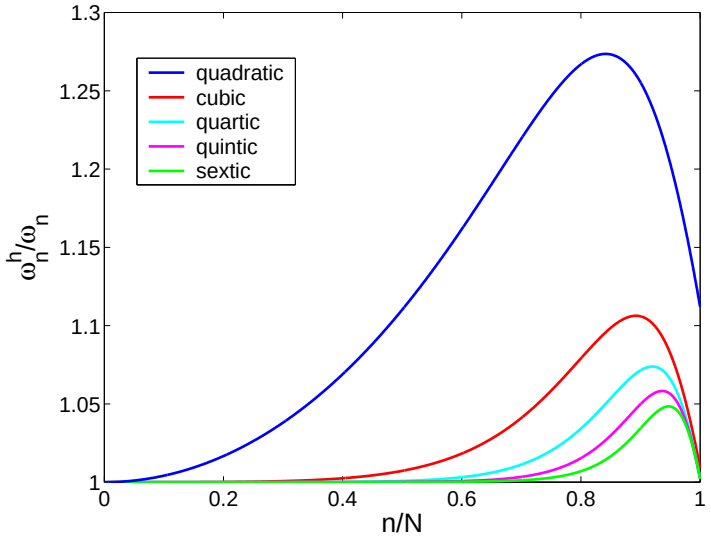

Figure 5.22: Beam problem: normalized discrete spectra using equally spaced control points.

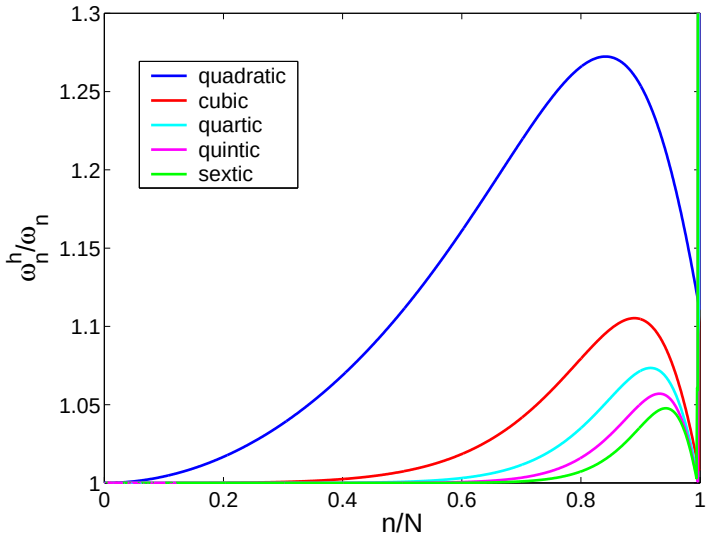

Figure 5.23: Cantilever beam with weak constraint imposition: normalized discrete spectra using different order NURBS basis functions.

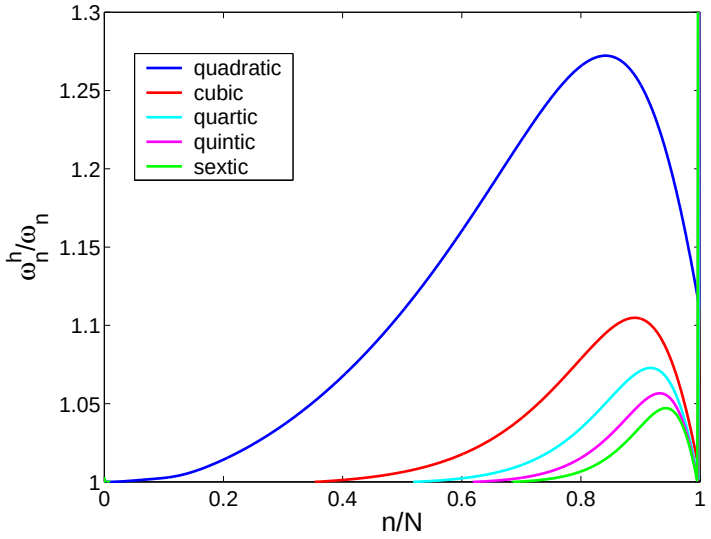

Figure 5.24: Cantilever beam with Lagrange multiplier: normalized discrete spectra using different order NURBS basis functions.

6. TWO-DIMENSIONAL PROBLEMS

In this Section I present some numerical experiments carried on over the 2D counterparts of the rod and the Euler-Bernoulli beam problems previously illustrated, which are respectively the transversal vibrations of an elastic membrane and of a Kirchhoff plate.

6.1 TRANSVERSAL VIBRATIONS OF AN ELASTIC MEMBRANE

The first problem I deal with consists of the study of the transversal vibrations of a simply-supported, square elastic membrane, whose natural frequencies and modes, assuming unit material parameters and edge length, are governed by the Laplace problem:

$$\begin{aligned} &\nabla^2 u(x,y) + \omega^2 u(x,y) = 0 \text{ for } (x,y) \in \Omega =]0,1[\times]0,1[\\ &u(x,y)|_{\partial\Omega} = 0. \end{aligned} \tag{6.1}$$

The exact solution in terms of natural frequencies (see for example Meirovitch (1967)) is:

$$\omega_{mn} = \pi\sqrt{m^2+n^2}, \text{ with } m,n = 1,2,3... \tag{6.2}$$

Also for this case, a problem of the form of (4.7) is obtained after the discretization of the weak formulation.

The numerical results are qualitatively similar to the ones obtained in the study of 1D problems. In Figure 6.1, I report the normalized discrete spectra obtained employing different order NURBS basis functions and using a linear parametrization over a 40×40 control net. Note that l is the number of modes sorted from the lowest to the highest in frequency, while N is the total number

of degrees-of-freedom. Moreover, in Figure 6.2 I show a zoom of the lower frequency half of the spectra to highlight the order of accuracy of the different approximations. Also in this case the method denotes a bad last part of the spectrum, wider than in 1D cases, but percentually decreasing as the number of control points increases. For this problem too, this bad behaviour can be avoided by means of an equally spaced control net as shown in Figure 6.3. Finally Figure 6.4 shows the average relative error over the spectra shown in Figure 6.3.

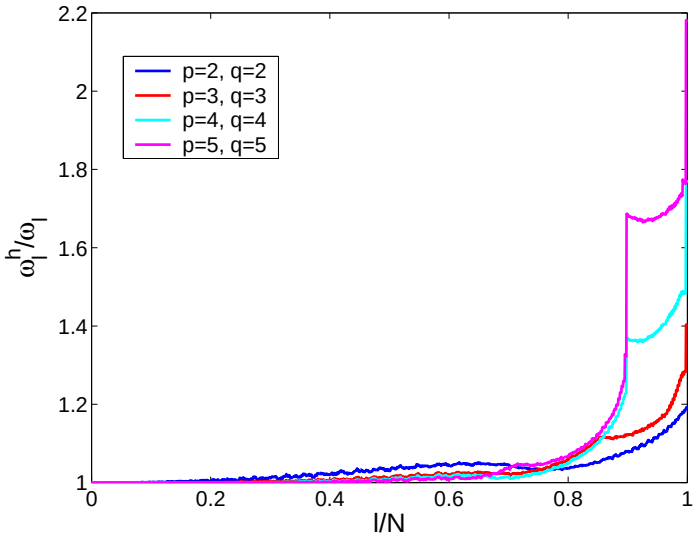

Figure 6.1: Membrane problem: normalized discrete spectra using different order NURBS basis functions (40×40 control points).

6.2 TRANSVERSAL VIBRATIONS OF A KIRCHHOFF PLATE

The second 2D problem studied is the analysis of the transversal vibrations of a simply-supported, square Kirchhoff plate. Its natural frequencies and modes, assuming unit flexural rigidity, density and edge length, are governed by the biharmonic problem:

$$\begin{aligned} &\nabla^4 u(x,y) - \omega^2 u(x,y) = 0 \text{ for } (x,y) \in \Omega =]0,1[\times]0,1[\\ &u(x,y)|_{\partial\Omega} = 0, \end{aligned} \tag{6.3}$$

for which the exact solution in terms of natural frequencies (see for example Meirovitch (1967)) is:

$$\omega_{mn} = \pi^2(m^2+n^2), \text{ with } m,n = 1,2,3... \tag{6.4}$$

Also this formulation gives rise to a problem of the form of (4.7).

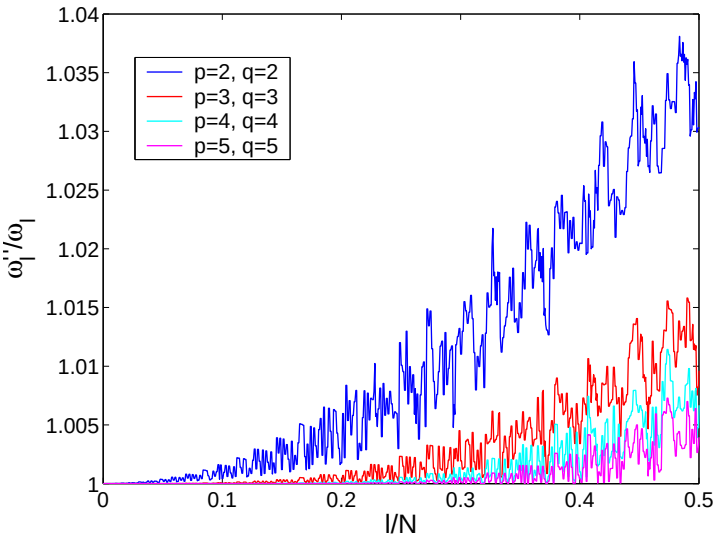

Figure 6.2: Membrane problem: zoom of the low frequency part of the normalized discrete spectra.

I remark that even in this case, as for the Euler-Bernoulli beam, my NURBS formulation results in a *rotation-free* approach. As proposed in Engel et al. (2002), the boundary conditions on rotations can be imposed in the same way previously discussed for the beam case.

The numerical results are analogous to the ones obtained for the elastic membrane. In Figure 6.5, I report the normalized discrete spectra using a linear parametrization over a 40×40 control net and in Figure 6.6 I show a zoom of their lower frequency part. Note that I have cut off the y-axis of the plot of Figure 6.5 to a value of 2.0 because otherwise the outlier frequencies for the highest order approximations would make the remaining part of the plot completely unreadable and useless. The same considerations done for the previous 2D example could be repeated, and in Figure 6.7 I show the spectra obtained employing an equally spaced control net. Finally, Figure 6.8 shows the average relative error computed over the spectra of Figure 6.7.

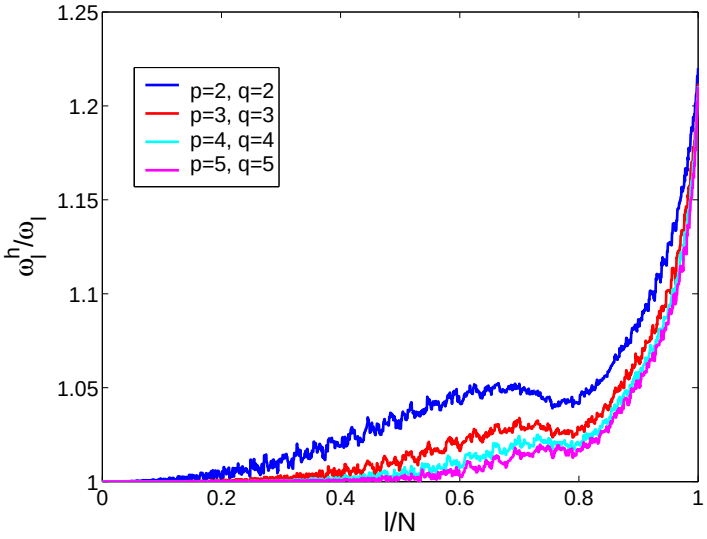

Figure 6.3: Membrane problem: normalized discrete spectra using an equally spaced control net.

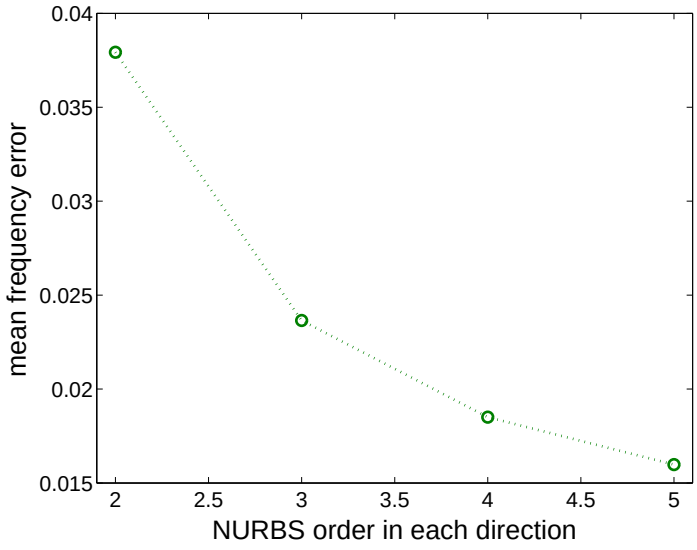

Figure 6.4: Membrane problem: average relative error of the spectra shown in Figure 6.3.

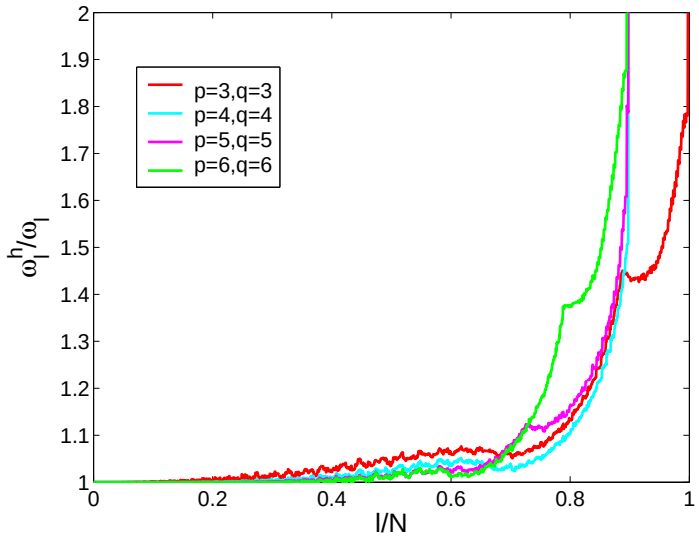

Figure 6.5: Plate problem: normalized discrete spectra using different order NURBS basis functions (40×40 control points).

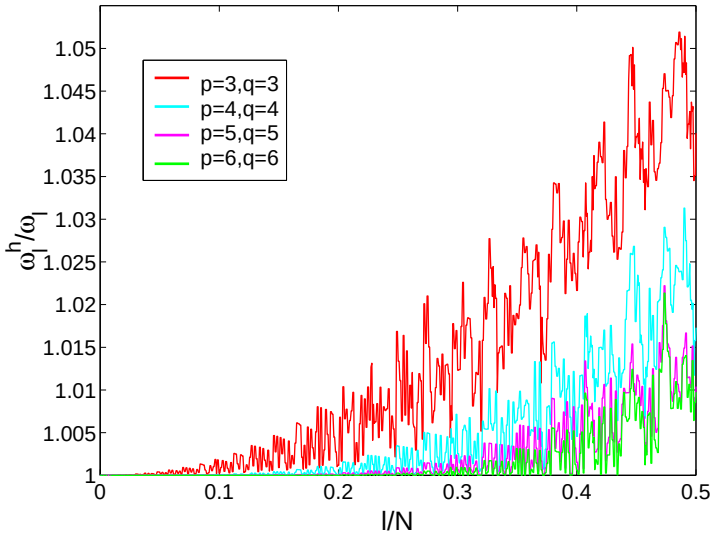

Figure 6.6: Plate problem: zoom of the low frequency part of the normalized discrete spectra.

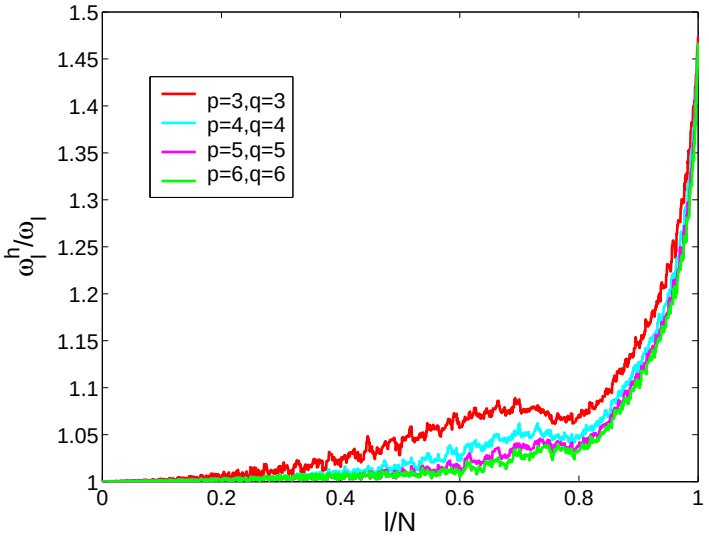

Figure 6.7: Plate problem: normalized discrete spectra using an equally spaced control net.

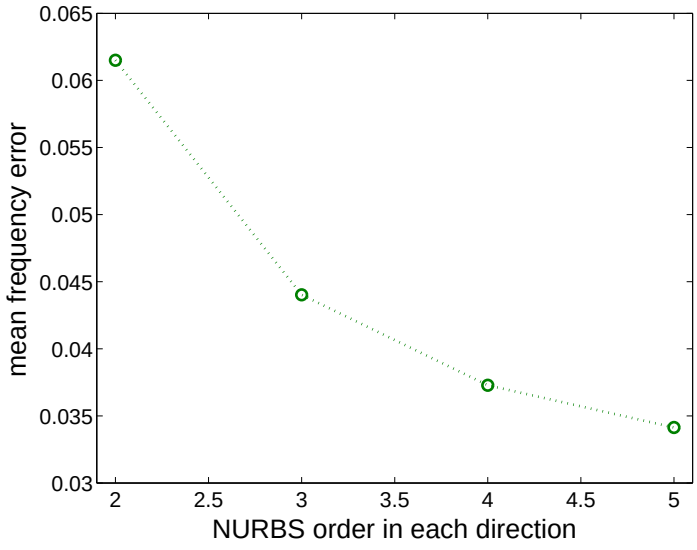

Figure 6.8: Plate problem: average relative error of the spectra shown in Figure 6.7.

7. VIBRATIONS OF A CLAMPED THIN CIRCULAR PLATE USING 3D SOLID ELEMENTS

One of the greatest advantages of Isogeometric Analysis is its capability of working in exact geometry even for coarse meshes. So, for instance, I can study with few NURBS elements a circular domain, and not a faceted polygonal one which only tends to be circular (for example a circle can be represented exactly by means of only three pieces of quadratic NURBS curves, as shown in their books by Piegl and Tiller (1997) and Rogers (2001)).
Another important feature of this technique, shown in the work of Hughes et al. (2004), is the fact that, employing the NURBS equivalent of classical finite element p-methods, it is possible to study thin structures like plates and shells with 3D solid elements.
In this framework, an interesting example is the study of the vibrations of a clamped thin circular plate. My approach has been to construct a coarse mesh (anyway capable to exactly reproduce geometry) and then to elevate the order of the basis functions until a sufficient precision in the approximation of the first three frequencies has been achieved. The exact solution for this problem under Kirchhoff's assumptions is presented, for example, in Meirovitch (1967) and is the following:

$$\omega_{mn} = C_{mn}^2 \frac{\pi^2}{R^2} \sqrt{\frac{D_E t}{\rho}} \, [rad/s], \tag{7.1}$$

where R is the radius of the plate, t is the thickness, $D_E = \dfrac{Et^3}{12(1-\nu^2)}$ is the flexural rigidity (being E and ν respectively the Young's modulus and the Poisson's ratio) and ρ is the density (mass per unit volume); for the first three frequencies the values of the coefficients C_{mn} are:

$$C_{01} = 1.015,\ C_{11} = 1.468 \text{ and } C_{02} = 2.007.$$

The data for the problem that I have studied are shown in Table 7.1, where concrete typical material parameters have been used. Note moreover that the radius to thickness ratio of 100 makes this problem a thin plate, for which Kirchhoff's assumptions can be considered valid.

The starting control net consists of $9 \times 4 \times 3$ control points and quadratic approximations in

R	2 $[m]$
t	.02 $[m]$
E	$30{\cdot}10^6$ $[KN/m^2]$
ν	.2
ρ	2.320 $[t/m^3]$

Table 7.1: Clamped circular plate: geometric and material parameters.

all the parametric directions are initially employed. Figure 7.1 shows the mesh, consisting in a very coarse 8 non-zero-volume element patch.

The numerical results as compared with the exact solution are reported in Table 7.2, where p, q and r are the orders of the basis functions in the circumferential, radial and vertical directions, respectively, and reveal the good behaviour of this kind of analysis for such a problem.

Moreover, Figures 7.2-7.4 show the shapes of the first three eigenmodes (computed using $p = 4$,

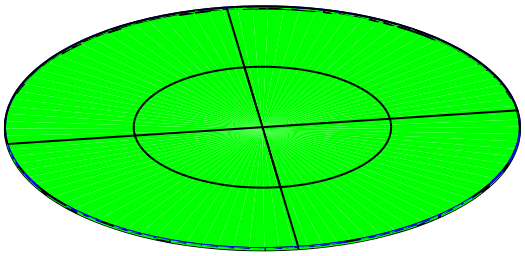

Figure 7.1: Clamped circular plate: 8 non-zero-volume element mesh.

p	q	r	ω_{01} $[rad/s]$	ω_{11} $[rad/s]$	ω_{02} $[rad/s]$
2	2	2	138.133	1648.800	2052.440
2	3	2	56.702	267.765	276.684
3	3	2	56.051	126.684	232.788
3	4	2	54.284	124.417	212.451
4	4	2	54.284	113.209	212.451
4	5	2	54.153	112.700	210.840
exact			53.863	112.670	210.597

Table 7.2: Clamped circular plate: numerical results as compared with the exact solution.

$q = 5$, $r = 2$ elements), which qualitatively agree with the ones depicted in Meirovitch (1967).

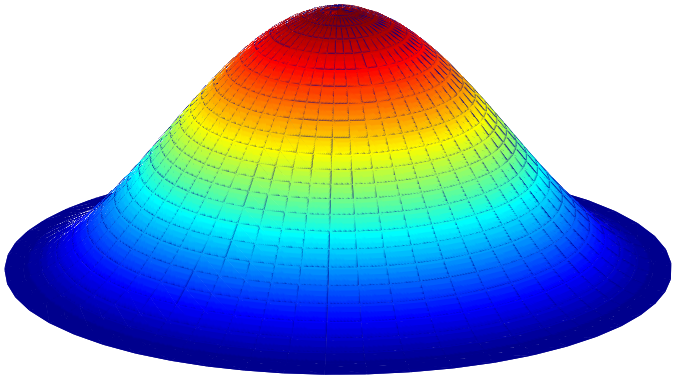

Figure 7.2: Clamped circular plate: eigenmode corresponding to ω_{01}.

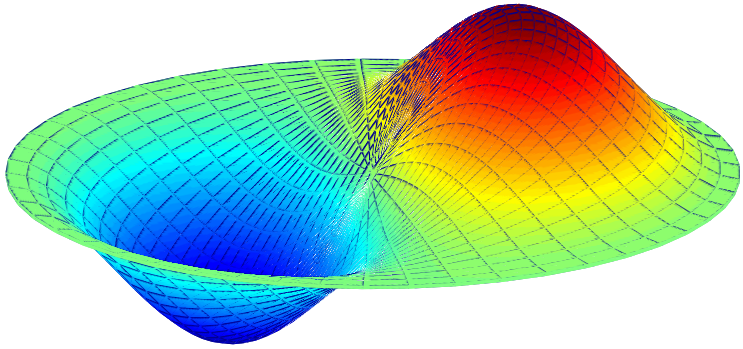

Figure 7.3: Clamped circular plate: eigenmode corresponding to ω_{11}.

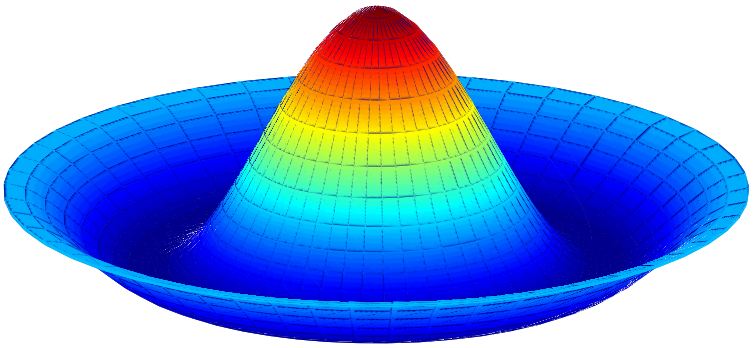

Figure 7.4: Clamped circular plate: eigenmode corresponding to ω_{02}.

8. CONCLUSIONS

In the present work the recently introduced (see Hughes et al. (2004)) concept of Isogeometric Analysis has been, for the first time, applied to the study of structural vibrations.

After a review of some basics of Non-Uniform Rational B-Splines and of the main ideas of Isogemetric Analysis, the determination of the structural frequencies for different problems has been performed by means of this new kind of analysis.
In particular one-dimensional problems, like rods and beams, and two-dimensional ones, like membranes and plates, have been studied.
The new method has shown very good results in all these cases and, when compared with analogous classical finite element results, it has shown a superior behaviour.
Another investigated issue has been the possibility of developing, in a natural way, rotation-free thin bending elements. The problem of the imposition of boundary conditions on rotations both weakly and with Lagrange multipliers has been discussed for rotation-free beam elements.
Finally the exact geometry property of the method has been exploited in order to study a three-dimensional circular problem. In the same example, the capability of the method to study thin bending structures (a plate in this case) by means of 3D solid elements has also been tested, obtaining very good results.

Since these preliminary results have shown that this technique could be very important in the framework of structural vibrations, more research in this context is needed for the future. Some issues could be deeper studies on different parametrizations (in particular to avoid the appearance of what have been called “outlier frequencies”, which are some strange too high frequencies at the very end of the discrete spectrum for higher order approximations) and on lumped mass

formulations. Moreover, the method needs to be tested in different cases of geometrically complicated real structures, where it promises to be very effective in particular as compared with standard finite element analysis.

A. COMPUTATION OF THE ISOGEOMETRIC ANALYSIS ORDER OF ACCURACY FOR THE ROD PROBLEM

Starting from the analytical expressions for the normalized discrete spectra obtained previously, it is possible to compute their order of accuracy by means of Taylor expansions.
In the following I show the computation of the order of accuracy for the rod problem using both consistent and lumped mass formulations and employing quadratic and cubic NURBS.

A.1 ORDER OF ACCURACY EMPLOYING QUADRATIC NURBS AND CONSISTENT MASS

The analytical expression for the normalized discrete spectrum in this case is:

$$\frac{\omega^h}{\omega} = \frac{1}{\omega h}\sqrt{\frac{20(2-\cos(\omega h)-\cos^2(\omega h))}{16+13\cos(\omega h)+\cos^2(\omega h)}}. \tag{A.1}$$

First I make use of the expansion $\cos(x) \sim 1 - x^2/2 + x^4/4! - x^6/6!$, obtaining after simple computations:

$$\frac{\omega^h}{\omega} \sim \frac{1}{\omega h}\sqrt{\frac{30(\omega h)^2 - \frac{15}{2}(\omega h)^4 + \frac{11}{12}(\omega h)^6}{30 - \frac{15}{2}(\omega h)^2 + \frac{7}{8}(\omega h)^4}}, \tag{A.2}$$

which can be rewritten as:

$$\frac{\omega^h}{\omega} \sim \sqrt{\frac{N}{D}} \tag{A.3}$$

with N and D defined as follows:

$$\begin{aligned} N &= 30 - \frac{15}{2}(\omega h)^2 + \frac{11}{12}(\omega h)^4, \\ D &= 30 - \frac{15}{2}(\omega h)^2 + \frac{7}{8}(\omega h)^4. \end{aligned} \tag{A.4}$$

Expression (A.3) can be written as:

$$\frac{\omega^h}{\omega} \sim \sqrt{\frac{1}{1 + \dfrac{D-N}{N}}} \tag{A.5}$$

and, using the expansions $\dfrac{1}{1+x} \sim 1 - x$ and $\sqrt{1-x} \sim 1 - x/2$, it gives rise to:

$$\frac{\omega^h}{\omega} \sim 1 + \frac{N-D}{2N}. \tag{A.6}$$

Finally, substituting the expressions (A.4) for N and D, I get that:

$$\frac{\omega^h}{\omega} \sim 1 + \frac{(\omega h)^4}{1440}, \tag{A.7}$$

which reveals that the order of accuracy is equal to 4.

Figure A.1 shows that, for low frequencies, the normalized discrete spectrum has the same behaviour of the function $1 + (\omega h)^4/1440$ (recall: $\omega h = \pi n / n_{el}$).

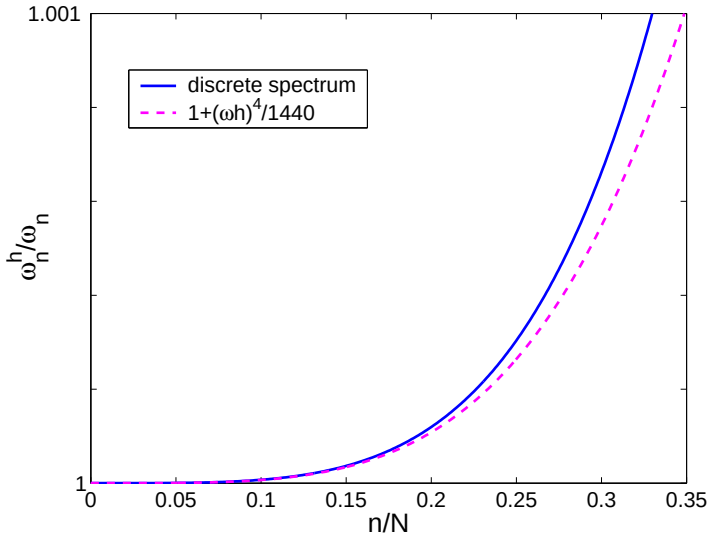

Figure A.1: Rod problem: normalized discrete spectrum using quadratic NURBS versus $1 + (\omega h)^4/1440$ for low frequencies.

A.2 ORDER OF ACCURACY EMPLOYING CUBIC NURBS AND CONSISTENT MASS

Using cubic NURBS, the normalized discrete spectrum is represented by:

$$\frac{\omega^h}{\omega} = \frac{1}{\omega h}\sqrt{\frac{42(16 - 3\cos(\omega h) - 12\cos^2(\omega h) - \cos^3(\omega h))}{272 + 297\cos(\omega h) + 60\cos^2(\omega h) + \cos^3(\omega h)}}. \tag{A.8}$$

Expanding $\cos(\omega h)$ and repeating the same computations as before, I obtain that:

$$\frac{\omega^h}{\omega} \sim 1 + \frac{(\omega h)^6}{60480}, \tag{A.9}$$

so the order of accuracy in this case is 6 and Figure A.2 confirms this result.

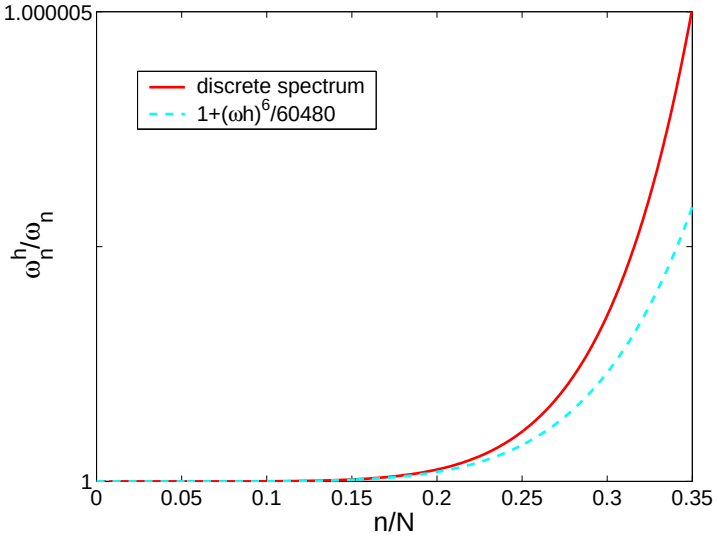

Figure A.2: Rod problem: normalized discrete spectrum using cubic NURBS versus $1 + (\omega h)^6/60480$ for low frequencies.

A.3 ORDER OF ACCURACY EMPLOYING LUMPED MASS

Similarly to what have been done in the case of consistent mass, also using a lumped mass formulation it is possible to compute the analytical expression for the discrete spectrum arising from the generic interior element equations. In this way, employing quadratic NURBS, I obtain:

$$\frac{\omega^h}{\omega} = \frac{1}{\omega h}\sqrt{\frac{2}{3}(2 - \cos(\omega h) - \cos^2(\omega h))}, \tag{A.10}$$

while with cubic NURBS we get:

$$\frac{\omega^h}{\omega} = \frac{1}{\omega h}\sqrt{\frac{1}{15}(16 - 3\cos(\omega h) - 12\cos^2(\omega h) - \cos^3(\omega h))}. \tag{A.11}$$

In this case, these analytical expressions do not reproduce the behaviour of (almost) the whole numerical spectra, but only of their part before the discontinuous derivative point, as shown in Figure A.3.

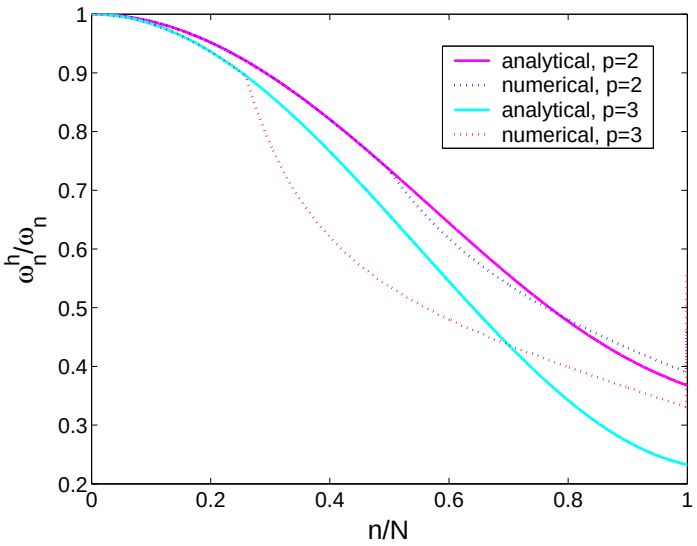

Figure A.3: Rod problem: analytical versus numerical discrete spectrum computed using quadratic and cubic NURBS; lumped mass formulation.

But when I compute the order of accuracy I am interested only in the very low frequency part of the spectrum, so I can carry on the same computation as before.
So, by means of Taylor expansions, I obtain, using quadratic NURBS:

$$\frac{\omega^h}{\omega} \sim 1 - \frac{(\omega h)^2}{8} \tag{A.12}$$

and using cubic NURBS:

$$\frac{\omega^h}{\omega} \sim 1 - \frac{(\omega h)^2}{6}. \tag{A.13}$$

I remark that, as it was already evident from Figure 5.13, by increasing the order p I do not achieve a better order of accuracy, which for lumped mass formulation is always equal to 2.
Finally Figures A.4 and A.5 confirm the validity of expressions (A.12) and (A.13), respectively.

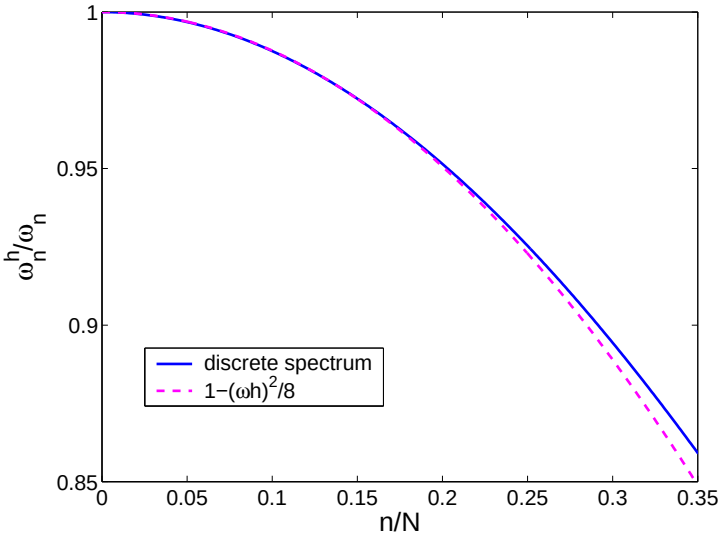

Figure A.4: Rod problem: normalized discrete spectrum using cubic NURBS versus $1-(\omega h)^2/8$ for low frequencies; lumped mass formulation.

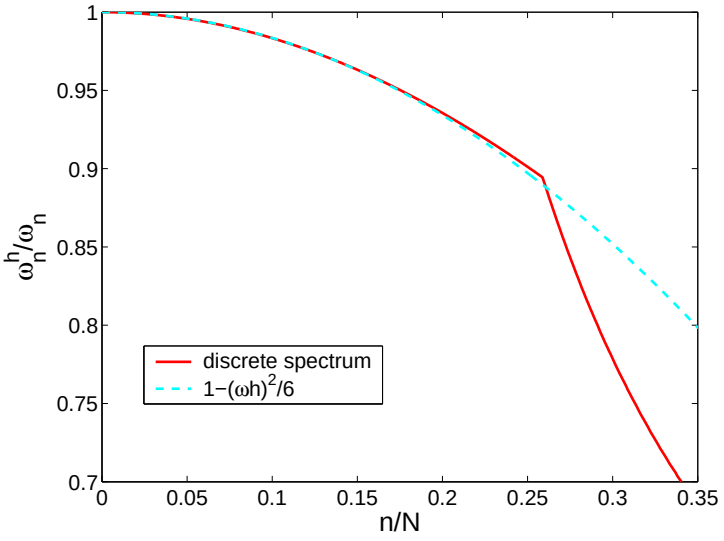

Figure A.5: Rod problem: normalized discrete spectrum using cubic NURBS versus $1-(\omega h)^2/6$ for low frequencies; lumped mass formulation.

Bibliography

Babuška, I. (1973). The Finite Element Method with Lagrange Multipliers. *Numerische Mathematik 20*, 179192.

Barbosa, H. J. C. and T. J. R. Hughes (1991). The Finite Element Method with Lagrange Multipliers on the Boundary: Circumventing the Babuška-Brezzi Condition. *Computer Methods in Applied Mechanics and Engineering 85*, 109–128.

Chopra, A. K. (2001). *Dynamics of Structures. Theory and Applications to Earthquake Engineering, Second Edition*. Prentice-Hall, Upper Saddle River, New Jersey.

Cirak, F., M. Ortiz, and P. Schröeder (2000). Subdivision Surfaces: a New Paradigm for Thin Shell Analysis. *International Journal for Numerical Methods in Engineering 47*, 2039–2072.

Cirak, F., M. J. Scott, E. K. Antonsson, M. Ortiz, and P. Schröeder (2002). Integrated Modeling, Finite-Element Analysis and Engineering Design for Thin Shell Structures using Subdivision. *Computer-Aided Design 34*, 137–148.

Clough, R. W. and J. Penzien (1993). *Dynamics of Structures*. McGraw-Hill, New York.

Engel, G., K. Garikipati, T. J. R. Hughes, M. G. Larson, L. Mazzei, and R. L. Taylor (2002). Continuous/Discontinuous Finite Element Approximations of Fourth-Order Elliptic Problems in Structural and Continuum Mechanics with Applications to Thin Beams and Plates, and Strain Gradient Elasticity. *Computer Methods in Applied Mechanics and Engineering 191*, 669–3750.

Fried, I. and D. S. Malkus (1976). Finite Element Mass Lumping by Numerical Integration Without Convergence Rate Loss. *International Journal of Solids and Structures 11*, 461–466.

Höllig, K. (2003). *Finite Element Methods with B-Splines*. SIAM, Philadelphia.

Hughes, T. J. R. (2000). *The Finite Element Method: Linear Static and Dynamic Finite Element Analysis*. Dover Publications, Mineola, New York.

Hughes, T. J. R., J. A. Cottrell, and Y. Bazilevs (2004). Isogeometric Analysis: CAD, Finite Elements, NURBS, Exact Geometry and Mesh Refinement. *Computer Methods in Applied Mechanics and Engineering*, to appear.

Hughes, T. J. R., H. M. Hilber, and R. L. Taylor (1976). A Reduction Scheme for Problems of Structural Dynamics. *International Journal of Solids and Structures 12*, 749–767.

Meirovitch, L. (1967). *Analytical Methods in Vibrations*. The MacMillan Company, New York.

Motulsky, H. (1995). *Intuitive Biostatistics*. Oxford University Press, New York.

Nitsche, J. A. (1971). Über ein Variationsprinzip zur Lösung von Dirichlet-Problemen bei Verwendung von Teilräumen, die keinen Randbedingungen unterworfen sind. *Abhandlungen aus dem Mathematischen Seminar der Üniversität Hamburg 36*, 9–15.

Oñate, E. and M. Cervera (1993). Derivation of Thin Plate Bending Elements with One Degree of Freedom per Node: a Simple Three Node Triangle. *Engineering Computations 10*, 543–561.

Oñate, E. and F. Zarate (2000). Triangular Plate and Shell Elements. *International Journal for Numerical Methods in Engineering 47*, 557–603.

Phaal, R. and C. R. Calladine (1992a). A Simple Class of Finite-Elements for Plate and Shell Problems. 1. Elements for Beams and Thin Flat Plates. *International Journal for Numerical Methods in Engineering 35*, 955–977.

Phaal, R. and C. R. Calladine (1992b). A Simple Class of Finite-Elements for Plate and Shell Problems. 2. An Element for Thin Shells with Only Translational Degrees of Freedom. *International Journal for Numerical Methods in Engineering 35*, 979–996.

Piegl, L. and W. Tiller (1997). *The NURBS Book, 2nd Edition*. Springer-Verlag, New York.

Prudhomme, S., F. Pascal, J. T. Oden, and A. Romkes (2001). A Priori Error Estimate for the Baumann-Oden Version of the Discontinuous Galerkin Method. *Comptes Rendus de l'Academie des Sciences I, Numerical Analysis 332*, 851–856.

Qin, H. and D. Terzopoulos (1996a). D-NURBS: a physics-based framework for geometric design. *IEEE Transactions on Visualization and Computer Graphics 2*, 85–96.

Qin, H. and D. Terzopoulos (1996b). Triangular NURBS and Their Dynamic Generalizations. *Computer-Aided Geometric Design 14*, 325–347.

Rogers, D. F. (2001). *An Introduction to NURBS With Historical Perspective*. Academic Press, San Diego, CA.

Timoshenko, S. and J. Goodier (1951). *Theory of Elasticity, Second Edition*. McGraw-Hill, New York.